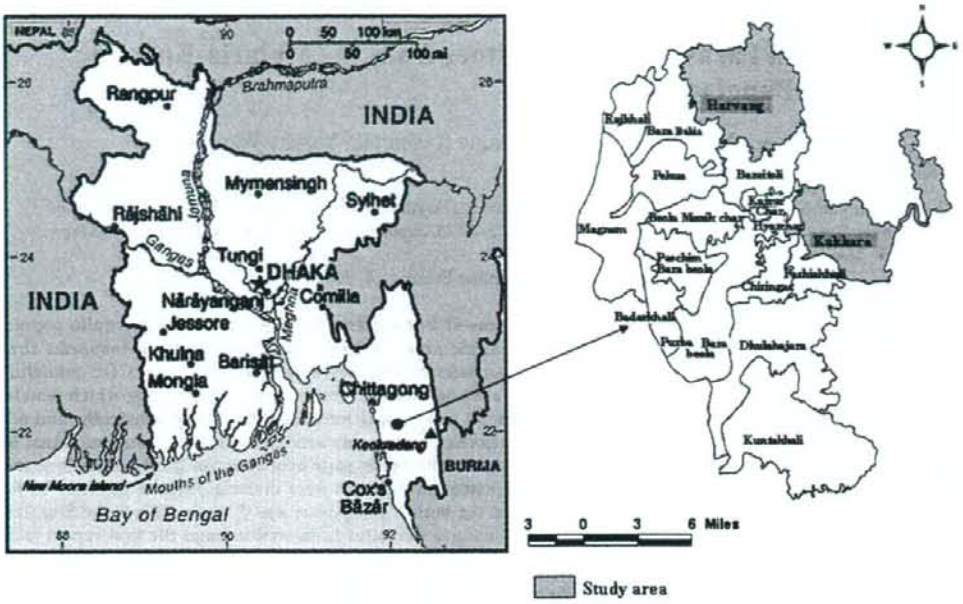

Fig. 1. Map of the Study Area Chakaria, Bangladesh, Where Mosquitoes Were Collected

Bangladesh, and the protocol was approved by the International Centre for Diarrhoeal Disease Research, Bangladesh (ICDDR, B). Chakaria is a subdivision in the district of Cox's Bazaar under the division of Chittagong. It has a population of 550000 with an area of 643.46 km^2, and is surrounded by many rivers such as the Matamuhuri, Maheshkhali, and Kutubdia Channel (Fig. 1). The east side of the Chakaria area is hilly with forests, and the west side is low lands bound by the Bay of Bengal. Two unions (Kakara and Harvang) of Chakaria were selected for mosquito collection. Traditionally, the main economic activities in the area have been agriculture, forestry, and fishing. Most of the people are very poor, wear very scanty clothes, and are exposed to the vector as they live in houses that sometimes have one or more side open. Household walls are usually made of bamboo and mud and very few are made of tin, wood, or cement; floors are earthen; roofs are made of leaves and straw and very few are of tin. The domesticated animals are cows, goats, and chickens that live in the areas surrounding houses. Cattle sheds are open without walls and located adjacent to households. The climate of Chakaria from May to September is characterized by heat and heavy rainfall, while the remainder of the year is mostly dry. The annual maximum temperature is 28—29 °C and the minimum temperature is 20—21 °C. Most rain occurs during the monsoon (June—September) and little in winter (November—February); annual rainfall is 3000—3500 mm. During the study period in June 2007, there was heavy rainfall of 425 mm/d in Chittagong division, and flooding made two-thirds of the area unreachable.

Mosquito Collection Adult mosquito collection was carried out June 12—30, 2007, just after the heavy rainfall. The mosquitoes were collected using six standard miniature CDC light traps (Model 512; John W. Hock Company, Gainesville, Florida, U.S.A.). In Chakaria, mosquitoes were collected from the three villages Goalmara, Pahartoli, and Manikpur in two unions upon receiving consent from the household heads. People living in these houses were protected with nonimpregnated bed nets. The trap was hung inside the room of sleeping persons as described previously.[24] The light traps were switched on each day at 18:00 and were collected at 06:00 of the next morning.

The captured mosquitoes were transported to the laboratory in plastic containers inside desiccators over silica gel. They were then separated into Culicinae and Anophelinae and counted. The individual female *Anopheles* mosquitoes were identified based on the taxonomic keys and stored in tubes inside the desiccators over silica gel until completely dry. The mosquitoes were stored under the same conditions until transported to the main laboratory, where they were stored at −80 °C until processed for DNA extraction.

Extraction of Malaria Parasite DNA from Mosquitoes DNA was extracted from the individual mosquitoes with MX-16 DNA purification kits (Promega, U.S.A.) that were used with the MX-16 instrument to provide an easy method for efficient automated purification of genomic DNA from solid biomaterials. This system is based on magnetic bead technology and composed of a magnetic bar, bore, and purified cartridge. In this system, the movement of the bore is controlled by motors, which allows easy DNA extraction from crude lysate magnetic beads. All the necessary reagents for purification of nucleic acid from a single mosquito are supplied in one reagent cartridge. Each well of the cartridge is prefilled with magnetic beads, wash buffer (I, GuSCN 5.25 M; II, 70% EtOH), and lysis buffer (GuSCN 4.7 M).[25] The DNA isolation was performed by adding sample into the lysis chamber. The procedures for DNA purification was performed automatically, and after DNA extraction it was transferred to a fresh tube and stored at −80 °C until use.

Target Sequences of Malaria Parasites The oligonuleotide primer set, biotin-labeled MPH1 of 5′-CAGATACCGTCGTAATCTTA-3′ and MPH2 of 5′-CCAAAGACTTTGATTTCTCAT-3′, which are specific to the 18Sr RNA genes of the human malaria parasites of *P. falciparum* and *Plasmodium vivax*, *Plasmodium ovale*, *Plasmodium ovale-variant*, and *Plasmodium malariae* were described previously.[20,23,26] These two primers were used for the DNA amplification of the malaria parasites in mosquitoes with PCR. After PCR amplification, the PCR products were used to distinguish the malaria parasite species using the MPH technique. The specific probes of *P. falciparum* 5′-GTCACCTCGAAAGATGACTT-3′, *P. vivax* 5′-TAAACTCCGAAGAGAAAATTC-3′, *P. ovale* 5′-AATTTCCCCGAAAGGAATTTTC-3′, *P. ovale-variant* 5′-GAAATTTCCAAAGGAATTTTC-3′, and *P. malariae* 5′-ACTCATATATAAGAATGTCTC-3′ were captured in the microtiter plate as described previously.[21,27]

Preparation of DNA for PCR Five microliters of extracted DNA from *Anopheles* mosquitoes was added to the 0.2 ml microcentrifuge tube containing 40 μl of lysis solution (Tris–HCl 110 mM, pH 8.9, $MgCl_2$ 1.5 mM, KCl 80 mM, BSA 500 μg/ml, 0.1% sodium cholate, 0.1% Triton X-100, Proteinase K 200 μg/ml, 0.45% Tween 20, 0.45% Nonidet p-40). Then the sample was incubated at 60 °C for 20 min for destruction and proteolysis, at 95 °C for 13 min to inactivate the Proteinase K, and then cooled at 50 °C for 5 min.

PCR and Electrophoresis PCR was carried out to detect the presence of malaria parasites in mosquitoes. The sample was spun down and mixed with 10 μl of PCR reagent mixture (Tris–HCl 10 mM, pH 8.9, $MgCl_2$ 1.5 mM, KCl 80 mM, BSA 500 μg/ml, 0.1% sodium cholate, 0.1% Triton X-100, 5 μg/ml primer, dNTPs 1 mM). The mixture was spun down, vortexed, and subjected to 30 cycles. The conditions were as follows: denaturation at 92 °C for 60 s, annealing at 52 °C for 90 s, and extension at 72 °C for 90 s. The amplified DNA was denatured by heating at 95 °C for 10 min and then rapid cooling on ice for 10 min. Positive controls were DNA of *P. falciparum*, *P. vivax*, *P. ovale*, *P. ovale-variant*, and *P. malariae* from clinical patients. Sterilized water was used as a negative control. The PCR products (10 μl) were electrophoresed at 100 V for 40 min using 1.2% agarose gel, stained by ethidium bromide, and the bands were visualized with a UV transillumintor.

Hybridization and Colorization of the MPH The procedure for hybridization and colorization in the MPH technique have been described previously.[23,26,28] Briefly, microtiter plate wells are coated with probes specific for *P. falciparum*, *P. vivax*, *P. ovale*, and *P. ovale-variant*, and *P. malariae* was added at 100 μl/well of 5×SSC (1×SSC is NaCl 0.15 M plus sodium citrate 0.015 M) and 5 μl of PCR product was added to the wells. Then the plate was incubated at 58 °C for 1 h, then the solution was removed, and the wells were washed three times with 250 μl/well of 1×solution (Tris–HCl 0.1 M, pH 7.5, NaCl 0.1 M, $MgCl_2$ 2 mM, 0.05% Triton X-100). Then 100 μl of alkaline phosphatase-labeled streptavidin was added and incubated at 28 °C for 15 min. After that the solution was removed and the well was washed three times with 250 μl/well of 1×solution. Then 100 μl/well of coloring substrate, PNPP solution (diethanolamine 1 M, pH 9.8, $MgCl_2$ 0.5 mM, and *para*-nitrophenyl phosphate 10 mM) were added and incubated at 28 °C for 30 min. The absorbance of each well was read at 405 nm using a microtiter plate reader (MPR-A4, Tosoh, Tokyo, Japan). The data were obtained by subtraction of the background corresponding to the PNPP solution.[20]

RESULTS

Proportion of Anopheline Mosquitoes Mosquitoes were captured only one time from each household of two unions in Chakaria during June 2007. In this survey, a total of 868 mosquitoes were collected from the three villages in two unions. Among the total collected mosquitoes, 669 (77.1%) mosquitoes were found to be female anopheline mosquitoes. The species of anopheline mosquitoes were morphologically identified as *A. minimus*, 651 (97.3%); 18 (2.7%) mosquitoes were other *Anopheles* species. The remaining 199 (22.9%) of the total collected mosquitoes were *Culex* species. Among the 868 mosquitoes, 838 were collected from the village of Pahartoli (Table 1).

Table 1. The Number of Mosquito Collected from Chakaria, Bangladesh (12—30 June, 2007)

Union name	Village name	Mosquito species			Total No.
		Anopheles minimus	Other *Anopheles* species	*Culex* species	
Harvang	Goalmara	0	4	17	21
Kakhara	Manikpur	2	7	0	9
	Pahartoli	649	7	182	838
Total		651 (75.0%)	18 (2.1%)	199 (22.9%)	868

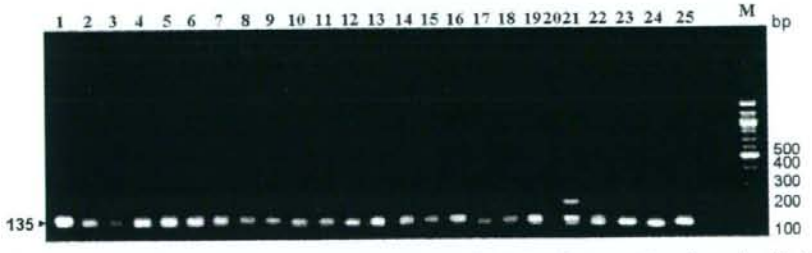

Fig. 2. Agarose Gel Electrophoresis Pattern Showing the Malaria Parasite-Positive PCR Product from *A. minimus* (Lanes 1—19), Negative Control (Lane 20), and Positive Control with DNA of *P. falciparum*, *P. vivax*, *P. ovale*, *P. ovale-variant*, and *P. malariae* (Lanes 21—25)

M, DNA ladder marker of 100 bp. PCR products represent the results of only malaria parasite-positive mosquitoes; malaria parasite-negative mosquitoes are not included.

Table 2. MPH Results of Mosquitoes Collected from Chakaria, Bangladesh (12—30 June, 2007)

Village name	Collection date	Total mosquito No.	*Plasmodium* species[a]			Total malaria positive No.
			Pf.	*Pv.*	*Pf.*+*Pv.*	
Goalmara	15th June	4	—	—	—	—
Pahartolir	15th June	25	—	—	—	—
Manikpur	20th June	9	—	—	—	—
Pahartoli	21st June	17	—	—	—	—
Pahartoli	22nd June	105	1	—	—	1
Pahartoli	23rd June	116	6	1	4	11
Pahartoli	24th June	85	—	—	—	—
Pahartoli	25th June	74	3	—	2	5
Pahartoli	26th June	84	—	—	—	—
Pahartoli	27th June	39	—	—	—	—
Pahartoli	28th June	24	1	—	—	1
Pahartoli	29th June	55	—	—	—	—
Pahartoli	30th June	32	1	—	—	1
Total		669	12	1	6	19

a) *Anopheles* mosquitoes which were positive of malaria parasites were *A. minimus*.

Table 3. Absorbance Value of Malaria Parasite Positive Mosquitoes by MPH

Mosquito no.	Collection date	Absorbance value at 405 nm[a]					*Plasmodium* species
		Pf.	*Pv.*	*Po.*	*Po-v.*	*Pm.*	
1	22nd June	0.625	0.005	0.008	0.007	0.007	*Pf.*
2	23rd June	0.468	0.011	0.011	0.005	0.011	*Pf.*
3	23rd June	0.304	0.675	0.000	0.000	0.006	*Pf.*+*Pv.*
4	23rd June	0.766	0.522	0.000	0.000	0.000	*Pf.*+*Pv.*
5	23rd June	0.780	0.986	0.004	0.000	0.000	*Pf.*+*Pv.*
6	23rd June	0.924	0.000	0.000	0.000	0.000	*Pf.*
7	23rd June	1.017	0.033	0.006	0.000	0.005	*Pf.*
8	23rd June	1.554	0.377	0.006	0.000	0.010	*Pf.*+*Pv.*
9	23rd June	1.121	0.080	0.019	0.000	0.022	*Pf.*
10	23rd June	0.000	0.392	0.003	0.000	0.005	*Pv.*
11	23rd June	0.513	0.000	0.004	0.000	0.004	*Pf.*
12	23rd June	0.575	0.000	0.000	0.000	0.000	*Pf.*
13	25th June	0.539	0.554	0.004	0.010	0.009	*Pf.*+*Pv.*
14	25th June	0.336	1.208	0.005	0.004	0.018	*Pf.*+*Pv.*
15	25th June	0.308	0.002	0.001	0.000	0.003	*Pf.*
16	25th June	0.612	0.002	0.006	0.000	0.019	*Pf.*
17	25th June	1.586	0.046	0.024	0.022	0.026	*Pf.*
18	28th June	1.370	0.020	0.019	0.017	0.012	*Pf.*
19	30th June	0.919	0.019	0.010	0.000	0.008	*Pf.*

a) Blank average for all reactions was 0.123 and all positive results were two times higher than the blank average. *Pf.*, *Plasmodium falciparum*; *Pv.*, *Plasmodium vivax*; *Po.*, *Plasmodium ovale*, *Po.-v.*, *Plasmodium ovale-variant*; *Pm.*, *Plasmodium malariae*.

Electrophoresis Results of PCR Product in Mosquitoes The extracted DNA of 669 mosquitoes was amplified using the primer pair set of MPH1 and MPH2 for detecting the malaria parasite. The amplified PCR product was subjected to agarose gel electrophoresis and this revealed a prominent band at 135 basepairs of malaria parasites in *Anopheles* mosquitoes. A total of 19 *Anopheles* mosquitoes were found to be malaria parasite positive (Fig. 2)

Results of MPH After PCR amplification, the PCR products were analyzed using the MPH technique. The total malaria parasite-positive rate was 2.8% (19/669) and it showed the same results as PCR. Among the 19 positive samples, 12 (63.2%) were positive only against the *P. falciparum* probe and 1 (5.3%) against the *P. vivax* probe. Six samples (31.6%) showed strong positive reactions against both the *P. falciparum* and *P. vivax* probe. Malaria parasite-positive mosquitoes were all *A. minimus* species and all were collected from the village of Pahartoli. Eleven malaria parasite-positive mosquitoes were collected on June 23, five on June 25, one on June 22, one on June 28, and one on June 30 (Table 2). The absorbance values of 19 samples of malaria-positive mosquitoes using the MPH technique are listed in Table 3.

DISCUSSION

Malaria vector surveillance is a prerequisite for malaria vector control. When vector surveillance is carried out on large numbers of mosquitoes, they must be tested for the presence of parasites. Salivary gland dissection is impractical when processing large numbers of mosquitoes.[17] Moreover, microscopic examination is time-consuming and labor intensive and cannot distinguish between different species of malaria parasites.[29] On the other hand, MPH is very sensitive

in distinguishing malaria parasite species. In Bangladesh, malaria is restricted to the hilly districts in the eastern and southern border areas.[30] Very few studies have been carried out in Bangladesh on the population densities of *Plasmodium* sporozoite-infected mosquitoes, especially in the endemic area of Chakaria, and the malaria infection rate in mosquitoes has not been determined. Therefore we tried to determine the malaria vector population infected with malaria parasites responsible for malaria transmission in the highly endemic area of Chakaria, Bangladesh. In the area, mosquito collection was conducted in June 2007, when there was unusually heavy rainfall and most of the study area was under water. Therefore it was difficult to collect *Anopheles* mosquitoes from all three villages, and most mosquitoes were collected from the village of Pahratoli.

In our study using CDC light traps, 77.1% of mosquitoes collected were anopheline, of which 97.3% were *A. minimus* mosquitoes. In another study, the mosquitoes were collected using the human landing aspiration technique, the anopheline mosquito collection rate was 37.0%, and among the *Anopheles* mosquitoes, *A. minimus* comprised 50% in the same area.[7] Other researchers reported that the *A. minimus* mosquito collection rate was 57.3% in the Chittagong Hill Tracts, which were also collected using human bait.[31] Data from our study suggest that rainfall may increase the *Anopheles* mosquito population. During the study, the Matamuhuri River surrounding the study area overflowed and may have increased the breeding area for *A. minimus*. The increase in population is related to the increase in breeding sites in which *Anopheles* eggs are deposited and develop into adults. Usually rainfall is associated with increased humidity that stimulates the resting gravid mosquitoes to oviposit and seek new hosts. In our study, the maximum number of mosquitoes was collected 2 weeks after the rainfall as it takes 10—14 d to mature after oviposition. The same result was found when numerous mosquitoes were concentrated in 2—4 weeks after rainfall.[32]

The sporozoite rate in mosquitoes can be detected using different methods such as the enzyme-linked immunosorbent assay (ELISA) and rapid dipstick immunochromatographic assay (Vec-Test Malaria). But ELISA requires training and with Vec-Test false-positive reactions may occur.[33,34] Nested PCR targeting 18S rRNA has also been used to detect malaria parasite infection in mosquitoes.[16] However, malaria parasites in mosquitoes are detected from a population pool, not from single mosquitoes, in these cases. Our study shows that malaria parasites can be identified from an individual female *Anopheles* using the MPH technique. Nineteen (2.8%) mosquitoes were found to be malaria positive. All were *A. minimus*, and the malaria parasite species in these mosquitoes were distinguished into 12 *P. falciparum*, one *P. vivax*, and six mixed infection with *P. falciparum* and *P. vivax*. It has been reported that mixed infection with *P. falciparum* and *P. vivax* was found in *A. dirus*, and mixed infection with *P. falciparum* and *P. malariae* was found in *Anopheles funestus* in Manchiana, Mozambique.[35,36] Khan and Talibi reported that the *A. minimus* sporozite rate was 1.3% in the Chittagong Hill Tracts, Bnagladesh,[31] one of the hilly areas in Bangladesh, and the sporozoites of *A. dirus* were indistinguishable but were assumed to be *P. vivax* or *P. falciparum*.[30] Malaria parasite-positive mosquitoes were also found in Chanpara, where the sporozoite rate was 2.3%, and Bagadi and Barakanda, where the sporozoite rate was 1.4%, all districts of in Dhaka.[3,4] In all cases, malaria parasites were detected by dissection of the salivary glands and parasite species were not identified. However, our study demonstrated that a simple technique can be used to isolate malaria parasite DNA from dried whole bodies of mosquitoes for PCR amplification and to distinguish malaria parasites using MPH. Therefore the MPH technique sensitively detects single and mixed infections with malaria parasites in *Anopheles* and both *P. falciparum* and *P. vivax* were predominant in the study area of Chakaria.

Our present findings show that 19 of 669 malaria parasite-positive *Anopheles* mosquitoes were detected, and that rate was higher than in the other study areas in Bangladesh. As malaria parasite DNA was extracted from the whole mosquitoes and not from the head and thorax, it cannot be confirmed that all the positive *Anopheles* mosquitoes could be involved in malaria parasite transmission. Further research may be required to detect malaria parasites-positive mosquitoes that can transmit malaria parasites. But our investigations revealed that the MPH technique is simple, sensitive, easy, and not time-consuming for malaria parasite detection in numerous mosquitoes. Our results also indicate that there may be a relation between rainfall and the *A. minimus* mosquito population. As one of the principal malaria vectors in Chakaria, *A. minimus* mosquitoes may play a greater role in malaria transmission in the area after heavy rainfall. Therefore special attention should be given to reducing the population of this mosquito for malaria control. This was the first report of distinguishing malaria parasites in individual female *Anopheles* mosquitoes using the MPH technique and also the first report of the malaria-positive rate in *Anopheles* in Chakaria, Bangladesh. The MPH technique is recommended for use in identifying malaria transmitters and in epidemiologic studies for promoting effective control measures not only for Bangladesh but also for other malaria-endemic areas. Our data will play an important role in initiating malaria control in Bangladesh.

Acknowledgments We thank Sk. Md. Shamsuzzaman and the field workers Md. Hamid, Md. Shahid, and staff of Chakaria Branch of the Centre for Health and Population Research ICDDR, B, Bangladesh for cooperating in this study. The ICDDR, B Research Centre support for this study is gratefully acknowledged. This work was supported in part by a Grant-in-Aid for Scientific Researchers on Priority Areas from the Ministry of Education, Culture, Sports, Science and Technology of Japan (19041049) and by the Programme for Promotion of Fundamental Studies in Health Sciences of the National Institute of Biomedical Innovation (NIBIO) (project no. 04-09, Yusuke Wataya).

REFERENCES

1) Levashina A. E., *Insect Biochem. Mol. Biol.*, **34**, 673—678 (2004).
2) Rahman A., Kogan F., Roytman L., *Am. J. Trop. Med. Hyg.*, **74**, 17—19 (2006).
3) Maheswary N. P., Habib M. A., Elias M., *Southeast Asian J. Trop. Med. Public Health*, **23**, 798—801 (1992).
4) Maheswary N. P., Khan Z., Molla F. R., Haq M. I., *Southeast Asian J. Trop. Med. Public Health*, **24**, 776—778 (1993).

5) Montanari R. M., Bangali A. M., Talukder K. R., Baqui A., Maheshwary N. P., Gosh A., Rahman M., Mahmood A. H., *Bull. World Health Org.*, **79**, 648—656 (2001).
6) Van den Broek I. V., Van der Wardt S., Talukdar L., Chakma S., Brockman A., Nair S., Anderson T. C., *Trop. Med. Int. Health*, **9**, 680—687 (2004).
7) ICDDR, B., *Health Sci. Bull.*, **1**, 10—14 (2003).
8) Blandin S. A., Levashina E. A., *Curr. Opin. Immunol.*, **16**, 16—20 (2004).
9) Ahmed T. U., *Mosq. Sys.*, **19**, 187—200 (1987).
10) Elias M., Dewan Z., Ahmed R., *J. Prev. Soc. Med.*, **1**, 20 (1982).
11) Lee H. W., Shin E., Cho S. H., Lee H., Kim C., Lee W., Moon S., Lee J., Lee W., Kim T., *Korean J. Parasitol.*, **40**, 75—81 (2002).
12) Mahapatra N., Marai N. S., Ranjit M. R., Parida S. K., Hansdah D. P., Hazra R. K., Kar S. K., *J. Vector Borne Dis.*, **43**, 191—194 (2006).
13) Stoffels J. A., Van Leeuwen W. M., Post R. J., *Med. Vet. Entomol.*, **19**, 433—437 (1995).
14) Moreno M., Cano J., Nzambo S., Bobuakasi L., Buatiche N. J., Ondo M., Micha F., Benito A., *Malaria J.*, **3**, 20 (2004).
15) Tassannakajon A., Boonsaeng V., Wilairat P., Panyim S., *Trans. R. Soc. Trop. Med. Hyg.*, **87**, 273—275 (1993).
16) Vythilingam I., Nitiavathy K., Yi P., Bakotee B., Hugo B., Singh B., Writz R. A., Palmer K., *Southeast Asian J. Trop. Med. Public Health*, **30**, 631—635 (1999).
17) Santos-Ciminera P. D., Achee N. L., Quinnan J. R., Roberts D. R., *J. Am. Mosq. Control Assoc.*, **20**, 165—271 (2003).
18) Harada M., Ishikawa H., Matsuoka H., Ishii A., Suguri S., *Acta Med. Okayama*, **54**, 165—171 (2000).
19) Ranford-Cartwright L. C., Balfe P., Carter R., *Mol. Biochem. Parasitol.*, **49**, 239—244 (1991).
20) Arai M., Kunisada K., Kawai S., Kimura M., Wataya Y., *Nucleosides Nucleotides*, **13**, 1363—1374 (1994).
21) Kawamoto F., Miyake H., Kaneko O., Kimura M., Nguyen T. D., Nguyen T. D., Liu Q., Zhou M., Le D. D., Kawai S., Isomura S., Wataya Y., *J. Clin. Microbiol.*, **34**, 2287—2289 (1996).
22) Laoboonchai A., Kawamoto F., Thanoosingha N., Kojima S., Scott-Miller R. R., Kain K. C., Wongsrichanalai C., *Trop. Med. Int. Health*, **6**, 458—462 (2001).
23) Chai J., Park Y., Guk S., Oh K., Oh M., Lee S., Kim H.-S., Wataya Y., *Am. J. Trop. Med. Hyg.*, **63**, 80—84 (2000).
24) Mboera L. E., Kihonda J., Braks M. A., Knols B. G., *Am. J. Trop. Med. Hyg.*, **59**, 595—596 (1998).
25) Ki J., Chang K., Roh H., Lee B., Yoon J., Jang G., *J. Biosci. Bioeng.*, **103**, 242—246 (2007).
26) Kimura M., Miyake H., Kim H.-S., Tanabe M., Arai M., Kawai S., Yamane A., Wataya Y., *J. Clin. Microbiol.*, **33**, 2342—2346 (1995).
27) Kawai S., Maekawajiri S., Yamane A., *Anal. Biochem.*, **209**, 63—69 (1993).
28) Arai M., Kunisada K., Kim H.-S., Miyake H., Mizukoshi C., Kakutani T., Yamane A., Nakagami S., Kawai S., Nakano H., Kawamoto F., Wataya Y., *Nucleosides Nucleotides*, **15**, 719—731 (1996).
29) Li F., Niu C., Ye B., *Chin. Med. J.*, **114**, 654—657 (2001).
30) Rosenberg R., Maheswary N. P., *Am. J. Trop. Med. Hyg.*, **31**, 183—191 (1982).
31) Khan A. Q., Talibi S. A., *Bull. World Health Org.*, **46**, 783—792 (1972).
32) Oesterholt M., Bousema J. T., Mwerinde O. K., Harris C., Lushino P., Masakoto A., Mwerinde H., Mosha F. W., Drakely C. J., *Malaria J.*, **5**, 98 (2006).
33) Writz R. A., Burkot T. R., Andre R. G., Rosenberg R., Collins W. E., Roberts D. R., *Am. J. Trop. Med. Hyg.*, **34**, 1048—1054 (1985).
34) Ryan J. R., Dave K., Coleman R. E., Emmerich E., Sattabongkot J., Dunton R. F., Writz R. A., *Med. Vet. Entomol.*, **15**, 225—230 (2001).
35) Rosenberg R., Andre R. G., Somchit L., *Trans. R. Soc. Trop. Med. Hyg.*, **84**, 22—28 (1990).
36) Marques P. X., Saute F., Pinto V. V., Cardoso S., Pinto J., Alonso P. L., Rosario do V. E., *Int. J. Biol. Sci.*, **2**, 96—102 (2005).

Bioorganic & Medicinal Chemistry 16 (2008) 7698–7704

Contents lists available at ScienceDirect

Bioorganic & Medicinal Chemistry

journal homepage: www.elsevier.com/locate/bmc

Synthesis and silencing properties of siRNAs possessing lipophilic groups at their 3′-termini

Yoshihito Ueno [a,b,d,f,*], Koshi Kawada [a], Tomoharu Naito [e], Aya Shibata [a], Kayo Yoshikawa [a], Hye-Sook Kim [e], Yusuke Wataya [e], Yukio Kitade [a,b,c,d,*]

[a] Department of Biomolecular Science, Faculty of Engineering, Gifu University, Medical Information Sciences, Gifu University, 1-1 Yanagido, Gifu 501-1193, Japan
[b] Center for Emerging Infectious Diseases, Gifu University, Medical Information Sciences, Gifu University, 1-1 Yanagido, Gifu 501-1193, Japan
[c] Center for Advanced Drug Research, Gifu University, Medical Information Sciences, Gifu University, 1-1 Yanagido, Gifu 501-1193, Japan
[d] United Graduate School of Drug Discovery and Medical Information Sciences, Gifu University, 1-1 Yanagido, Gifu 501-1193, Japan
[e] Faculty of Pharmaceutical Sciences, Okayama University, Tsushima, Okayama 700-8530, Japan
[f] PRESTO, JST (Japan Science and Technology Agency), 4-1-8 Honcho Kawaguchi, Saitama 332-0012, Japan

ARTICLE INFO

Article history:
Received 15 May 2008
Revised 2 July 2008
Accepted 3 July 2008
Available online 9 July 2008

Keywords:
RNAi
siRNA
Palmitic acid
Oleic acid
Cholesterol

ABSTRACT

Short-interfering RNAs (siRNAs) conjugated with lipophilic groups at their 3′-termini were synthesized. The properties of the synthesized siRNAs were examined in detail, and it was found that at low concentrations, their silencing abilities were dependent on the positions of the modifications and the types of organic molecules attached. Although the modification of siRNAs with palmitic acid or oleic acid at the 3′-end slightly reduced their silencing activities, siRNAs had enough abilities to induce RNAi at 10 nM concentrations. On the other hand, the modification of siRNAs with cholesterol at the 3′-end of the passenger strand was tolerated; however, the modification at the guide strand significantly reduces its silencing activity. The siRNAs modified with the lipophilic groups did not possess ability to penetrate the plasma membranes of HT-1080 cells without the transfection reagent. However, the results described in this report will aid in designing novel siRNAs with cell membrane-permeable molecules.

1. Introduction

Since the discovery of RNA interference (RNAi) as a means to silence expression of specific genes, small-interfering RNAs (siRNAs) have attracted significant attention as powerful tools for targeting therapeutically important mRNAs and eliciting their cleavage.[1,2] siRNA has considerable potential as a new therapeutic drug for intractable diseases because siRNAs can be logically designed and synthesized if the sequences of disease-causing genes are known. One of the critical problems in RNAi-based therapeutic applications is the delivery of siRNA across plasma membranes of cells in vivo. Thus far, a number of solutions to this problem have been reported.[3–9] Among them, the direct chemical modification of siRNAs is an attractive proposition because various kinds of organic molecules, which are specifically uptaken in specific tissues, can be specifically introduced into siRNAs. Recently, Soutschek et al. have succeeded in reducing plasma low-density lipoprotein (LDL) levels in mice by using siRNAs that are modified with cholesterol at the 3′-end of the guide strand (antisense strand).[4]

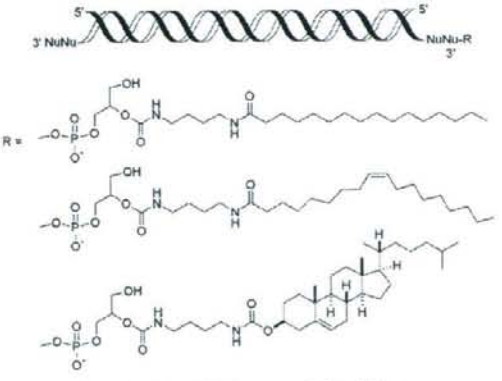

Figure 1. Structures of siRNAs possessing lipophilic groups.

It is deduced that the ability of siRNAs to induce RNAi depends on the positions of modifications and kinds of organic molecules attached. However, the silencing activities of siRNAs modified with

* Corresponding authors. Tel.: +81 58 293 2639; fax: +81 58 230 1893.
E-mail addresses: uenoy@gifu-u.ac.jp (Y. Ueno), ykkitade@gifu-u.ac.jp (Y. Kitade).

0968-0896/$ - see front matter © 2008 Elsevier Ltd. All rights reserved.
doi:10.1016/j.bmc.2008.07.010

cell membrane-permeable molecules have not been investigated systematically. In this paper, we report the synthesis and silencing properties of siRNAs possessing lipophilic groups at their 3′-termini (Fig. 1).

Argonaute2, a key component of RNA-induced silencing complex (RISC), is responsible for mRNA cleavage in the RNAi pathway.[10] Argonaute2 is composed of PAZ, Mid, and PIWI domains. The X-ray structural analysis of a co-crystal between a PIWI protein and an siRNA reveals that the 5′-phosphate of a guide strand (antisense strand) of siRNA is recognized by the PIWI domain and that the 5′-phosphate interacts with the carboxyl group of a C-terminal residue of the domain through a divalent metal ion.[11,12] It is observed that the modification of the 5′-hydroxyl groups of the guide strands of siRNAs by methoxy groups completely hampers the functions of siRNAs to induce RNAi in experiments using *Drosophila* embryo lysate and HeLa cell extract.[13,14] These results imply that the 5′-terminus of a guide strand is not suitable for modification by lipophilic groups.

On the other hand, X-ray structural analysis and a nuclear magnetic resonance (NMR) study have revealed that the 3′-overhang region of a guide strand of siRNA is recognized by the PAZ domain and the 2-nucleotide (nt) 3′-overhang is accommodated into a binding pocket composed of hydrophobic amino acids in the domain.[15–18] The length of the 3′-overhang regions of siRNA influences the activities of siRNAs. It is reported that the 2-nt 3′-overhang is the most efficient in an experiment using 21-nt siRNA in *Drosophila* embryo lysate; however, the multiple addition of 2′-deoxynucleotide to the 3′-end of siRNAs is tolerated.[19] On the basis of this information, we introduced lipophilic groups at the 3′-ends of the passenger or guide strands of siRNAs.

2. Results and discussion

Soutschek et al. used 4-hydroxyprolinol as a linker for conjugating RNAs and lipophilic groups. We selected glycerol, which was more flexible than hydroxyprolinol, as a linker to join RNAs and lipophilic groups. Glycerol derivative **1**[20] with 4,4′-dimethoxytrityl (DMTr) and *tert*-butyldimethylsilyl (TBDMS) groups at primary hydroxyls was synthesized according to the reported method, converted into its *O*-carbonylimidazolide, and reacted with 1,4-diaminobutane to afford an aminobutylcarbamoyl derivative **2** in 94% yield (Scheme 1). Palmitic acid and oleic acid were introduced into **2** in the presence of 1-ethyl-3-(3-dimethylaminopropyl)carbodiimide hydrochloride (WSCI) to yield glycerol derivatives **3** and **4** with fatty acids in 69% and 86% yields, respectively. On the other hand, cholesterol was converted into its *O*-carbonylimidazolide, which was then reacted with **2** to afford a cholesterol-modified glycerol **5** in 64% yield. After the desilylation of **3**, **4**, and **5** by tetrabutylammonium fluoride (TBAF), hydroxyl derivatives **6**, **7**, and **8** were succinated to give the corresponding succinates. They were linked to a controlled pore glass (CPG) to produce solid supports **9**, **10**, and **11** containing **6** (28 μmol/g), **7** (83 μmol/g), and **8** (88 μmol/g), respectively.

All oligoribonucleotides (ONs) were synthesized using solid supports **9**, **10**, and **11** by using a DNA/RNA synthesizer (Table 1). Fully protected ONs (1.0 μmol each) linked to solid supports were treated with concentrated NH_4OH/EtOH (3:1, v/v) at room temperature for 12 h and then with 1.0 M TBAF/THF at room temperature for 12 h. Released ONs were purified by denaturing 20% polyacrylamide gel electrophoresis (20% PAGE) to afford deprotected ONs **25–44**. These ONs were analyzed by matrix-assisted laser desorption/ionization time-of-flight mass spectrometry (MALDI-TOF/MS), and observed molecular weights were in agreement with their structures.

The ability of modified siRNAs to suppress gene expression was studied by a dual-luciferase assay using a psiCHECK-2 vector, which contained *Renilla* and firefly luciferase genes. Sequences of siRNAs were designed to target *Renilla* luciferase. HeLa cells were co-transfected with the vector and indicated amounts of siRNAs. Signals of *Renilla* luciferase were normalized to that of firefly

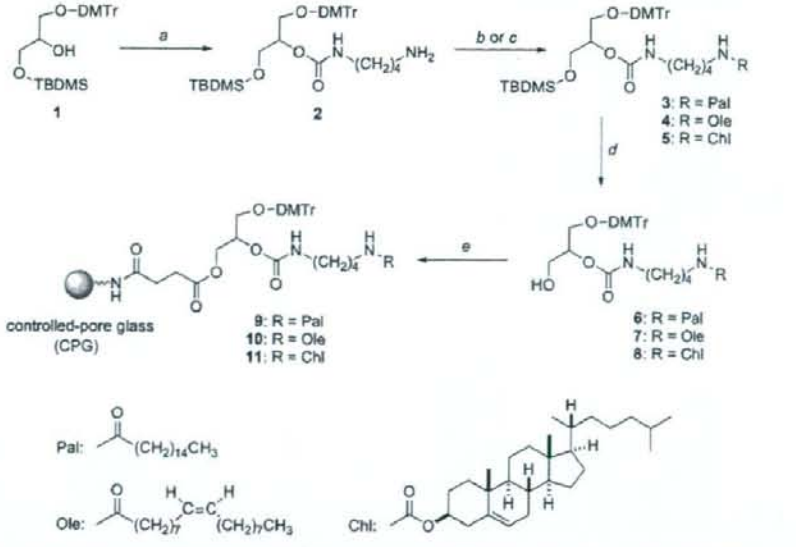

Scheme 1. Reagents and conditions: (a) (1) *N,N′*-carbonyldiimidazole, pyridine, rt, 1 h; (2) 1,4-diaminobutane, pyridine, rt, 3 h, 94%; (b) palmitic acid or oleic acid, WSCI, CH_2Cl_2, rt, 24 h, 69% for **3** and 64% for **4**; (c) cholesterol, *N,N′*-carbonyldiimidazole, pyridine, rt, 24 h, 64%; (d) TBAF, THF, rt, 80% for **6**, 82% for **7**, and 53% for **9**; (e) (1) succinic anhydride, DMAP, pyridine, rt, 24 h; (2) CPG, WSCI, DMF, rt, 72 h, 28 μmol/g for **9**, 83 μmol/g for **10**, and 88 μmol/g for **11**.

Table 1
Sequences of ONs and siRNAs used in this study

No. of siRNA	No. of ON	Sequence
siRNA12	ON25	5′-GGCCUUUCACUACUCCUACtt-3′
	ON26	3′-ttCCGGAAAGUGAUGAGGAUG-5′
siRNA13	ON27	5′-GGCCUUUCACUACUCCUACtt-3′-**Pal**
	ON26	3′-ttCCGGAAAGUGAUGAGGAUG-5′
siRNA14	ON28	5′-GGCCUUUCACUACUCCUACtt-3′-**Ole**
	ON26	3′-ttCCGGAAAGUGAUGAGGAUG-5′
siRNA15	ON29	5′-GGCCUUUCACUACUCCUACtt-3′-**Chl**
	ON26	3′-ttCCGGAAAGUGAUGAGGAUG-5′
siRNA16	ON25	5′-GGCCUUUCACUACUCCUACtt-3′
	ON30	**Pal**-3′-ttCCGGAAAGUGAUGAGGAUG-5′
siRNA17	ON25	5′-GGCCUUUCACUACUCCUACtt-3′
	ON31	**Ole**-3′-ttCCGGAAAGUGAUGAGGAUG-5′
siRNA18	ON25	5′-GGCCUUUCACUACUCCUACtt-3′
	ON32	**Chl**-3′-ttCCGGAAAGUGAUGAGGAUG-5′
siRNA19	ON33	5′-UUCUCCGAACGUGUGCACGUtt-3′
	ON34	3′-ttAAGAGGCUUGCACAGUGCA-5′
siRNA20	ON35	5′-AGAUCCAUACGUCCGUGAAtt-3′
	ON36	3′-ttUCUAGGUAUGCAGGCACUU-5′
siRNA21	ON37	5′-GCACCGGCAGGAGAUCAUAtt-3′
	ON38	3′-gtCGUGGCCGUCCUCUAGUAU-5′
siRNA22	ON39	5′-GCUGUUCAAAACGAAGAUGtt-3′-**Pal**
	ON40	**Pal**-3′-ttCGACAAGUUUUGCUUCUAC-5′
siRNA23	ON41	5′-GCUGUUCAAAACGAAGAUGtt-3′-**Ole**
	ON42	**Ole**-3′-ttCGACAAGUUUUGCUUCUAC-5′
siRNA24	ON43	5′-GCUGUUCAAAACGAAGAUGtt-3′-**Chl**
	ON44	**Chl**-3′-ttCGACAAGUUUUGCUUCUAC-5′

The capital letters indicate ribonucleosides. Small italic letters represent 2′-deoxyribonucleosides.

luciferase. The silencing activities of siRNAs correlated with the positions of the modifications and kinds of lipophilic groups attached at the 3′-termini of siRNAs (Fig. 2a and b). Although the modifications of passenger strands (sense strands) by palmitic acid and oleic acid reduced the silencing activities of siRNAs by a small amount as compared to that of unmodified siRNA, siRNAs modified with these fatty acids maintained their abilities to down-regulate protein expression levels to 30% at 10 nM concentrations. The silencing activity of siRNA modified with cholesterol at the 3′-end of the passenger strand was weaker than those of siRNAs modified with palmitic acid and oleic acid at each concentration. However, it down-regulated protein expression level to approximately 50% at 10 nM concentrations. The tendency of the silencing activities of siRNAs modified with palmitic acid and oleic acid at the 3′-ends of guide strands was similar to that of siRNAs modified at the 3′-ends of guide strands. On the other hand, the modification of siRNA with cholesterol at the 3′-end of the guide strand significantly reduced its silencing activity.

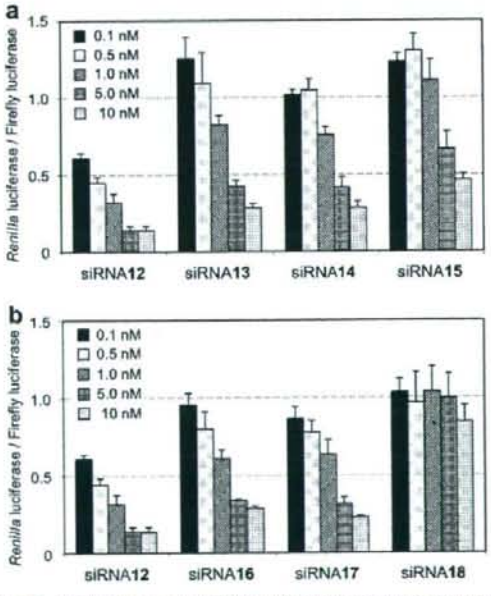

Figure 2. Dual-luciferase assay. (a) siRNAs modified at 3′-ends of passenger (sense) strands. (b) siRNAs modified at 3′-ends of guide (antisense) strands.

Argonaute2/eIF2C2 (hAgo2) has been identified as a key protein with an endonuclease activity associated with RISC in the RNAi pathway.[21,22] In order to examine whether or not the observed silencing activities could be attributed to RNAi, the activities of modified siRNAs were studied after treating HeLa cells with eIF2C2-targeting siRNAs. We considered that if the silencing activities of modified siRNAs resulted from RNAi, the expression levels of luciferase proteins would recover by treating HeLa cells with siRNAs targeting eIF2C2. Two kinds of siRNAs targeting eIF2C2—one (siRNA**20**) targeted open reading frame (ORP) positions 1168–1188 and the other (siRNA**21**) targeted ORP positions 1897–1917—were used in this study. The siRNA**19** is composed of a random sequence. HeLa cells were transfected with the siRNA**19**, **20** or **21**. After incubating them for 1 h, the cells were co-transfected with a psiCHECK-2 vector and siRNAs modified with lipophilic groups. After incubating for 24 h, the activities of *Renilla* luciferase were measured. The siRNA**19** composed of a random sequence did not largely change the expression level of *Renilla* luciferase (Fig. 3) whereas the signals of *Renilla* luciferase were recovered by treating them with siRNAs targeting eIF2C2 (Fig. 4). These results indicated that the silencing activities of modified siRNAs were attributed to RNAi.

In order to examine whether or not the siRNAs modified with the lipophilic groups can cross plasma membranes of cells without a transfection reagent, next, we performed an experiment targeting an endogenous protein. We chose an mRNA of a human RNase L protein, which is a constituent of the 2-5A system, as a target. It

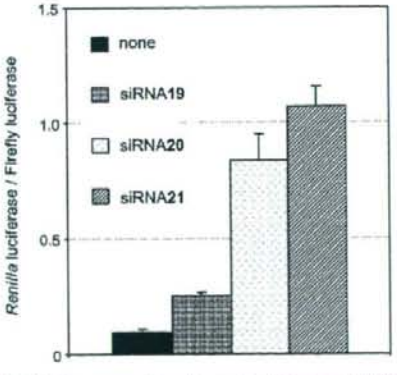

Figure 3. Dual-luciferase assay. HeLa cells were transfected with siRNA**19** (50 nM), siRNA**20** (50 nM), or siRNA**21** (50 nM). After incubating for 1 h, the cells were co-transfected with a psiCHECK-2 vector and siRNA**12** (10 nM). After incubating for 24 h, the activities of *Renilla* luciferase were measured.

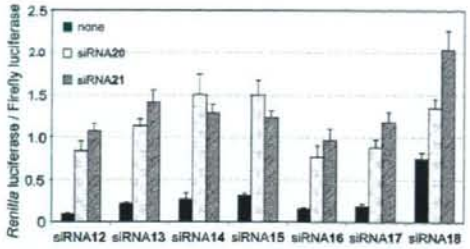

Figure 4. Dual-luciferase assay. HeLa cells were transfected with siRNA**20** (50 nM) or siRNA**21** (50 nM). After incubating for 1 h, the cells were co-transfected with a psiCHECK-2 vector and siRNAs (10 nM) modified with lipophilic groups. After incubating for 24 h, the activities of *Renilla* luciferase were measured.

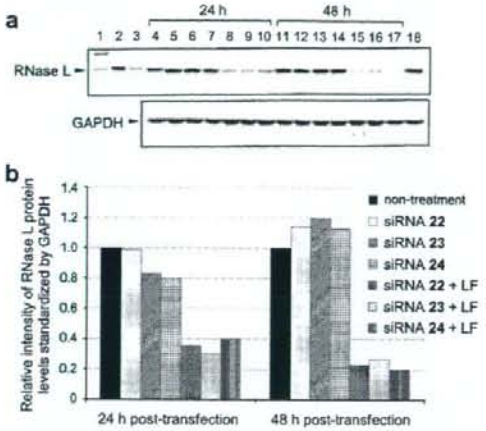

Figure 5. (a) Western blot analysis for human RNase L and GAPDH. Lanes 5–7 and 12–14, without Lipofectamine 2000; lanes 8–10 and 15–17, with Lipofectamine 2000. Lane 1, marker; lane 2, 3.5 ng RNase L; lane 3, 1.75 ng RNase L; lanes 4 and 11, non-treatment; lanes 5, 8, 12, and 15, siRNA **22**; lanes 6, 9, 13, and 16, siRNA23; lanes 5, 8, 12, and 15, siRNA**22**; lanes 7, 10, 14, and 17, siRNA**24**; lane 18, cells + 1.75 ng RNase L. (b) Relative intensities of RNase L protein levels standardized by GAPDH. LF indicates Lipofectamine 2000.

was reported that the absence of RNase L in vivo causes both a deficiency in the antiviral activity of interferon and a major defect in apoptosis[23,24]. We selected 23-nt of the open reading frame (ORP) position 94–112, that starts with 5′-AA-3′ and ends with 5′-TT-3′, as a target sequence. Sequences of the siRNAs are listed in Table 1. The siRNAs **22**, **23**, and **24** have palmitic acid, oleic acid, and cholesterol at the 3′-ends both of the passenger and guide strands, respectively.

HT-1080 human fibrosarcoma (HT-1080) cells were transfected with the siRNAs (200 nM concentrations) with and without the transfection reagent, and the cell lysates were analyzed 24 and 48 h later by immunoblot analysis with RNase L-specific antibody. Glyceraldehyde-3-phosphate dehydrogenase (GAPDH) protein level served as a loading control. The results of the immunoblot analysis are represented in Figure 5a. Figure 5b shows the relative intensities of RNase L protein levels standardized by GAPDH.

When the cells were transfected with the siRNAs **22**, **23**, and **24** by using the transfection reagent, the human RNase L protein expression levels were reduced to ~30% and ~20% at 24 and 48 h post-transfections, respectively. Thus, it was found that the modified siRNAs had the abilities to down-regulate the expression of the target protein. On the other hand, when the cells were treated with the abovementioned siRNAs without the transfection reagent, the expression levels of the human RNase L protein hardly changed at both 24 and 48 h post-transfections. From these results, it was revealed that the siRNAs modified with palmitic acid, oleic acid, and cholesterol did not have abilities to penetrate the plasma membranes of HT-1080 cells without the transfection reagent.

In conclusion, we have demonstrated the synthesis of siRNAs possessing lipophilic groups at their 3′-termini. It was found that all the modified siRNAs had similar silencing abilities at high siRNA concentrations but the silencing abilities of the modified siRNAs at low siRNA concentrations were dependent on the kind and positions of the modifications. Although the modifications of siRNAs with palmitic acid or oleic acid at their 3′-end reduced their silencing activities by a small amount, siRNAs had enough abilities to induce RNAi at their 10 nM concentrations. On the other hand, the modification of siRNA with cholesterol at the 3′-end of the passenger strand was tolerated; however, the modification at the guide strand significantly reduces its silencing activity. From these results, it is concluded that the 3′-end of the passenger strand is better than the guide strand for conjugating bulky molecules such as fatty acids, particularly rigid molecules such as cholesterol. The siRNAs modified with the lipophilic groups did not have abilities to penetrate the plasma membranes of HT-1080 cells without the transfection reagent. However, we believe that the results described here will aid in designing novel siRNAs with cell-membrane-permeable molecules.

3. Experimental

3.1. General remarks

NMR spectra were recorded at 400 MHz (^{1}H) and at 100 MHz (^{13}C), and are reported in parts per million downfield from tetramethylsilane. Coupling constants (*J*) are expressed in Hertz. Mass spectra were obtained by fast atom bombardment (FAB). Thin-layer chromatography was carried out on Merck-coated plates 60 F_{254}. Silica gel column chromatography was carried out on Wako gel C-300. siRNAs directed against eIF2C2 (hAgo2) were purchased from Qiagen Inc.

3.1.1.1-*O*-(4,4′-Dimethoxytrityl)-2-*O*-[*N*-(4-aminobutyl)carbamoyl]-3-*O*-tert-butyldimethylsilylglycerol (2)

A mixture of 1-*O*-(4,4′-dimethoxytrityl)-3-*O*-*tert*-butyldimethylsilylglycerol (**1**) (2.60 g, 5.11 mmol) and *N*,*N*′-carbonyldiimidazole (1.66 g, 10.2 mmol) in pyridine (17 mL) was stirred at room temperature. After 1 h, 1,4-diaminobutane (2.63 g, 29.8 mmol) was added to the mixture at 0 °C, and the whole was stirred at room temperature. After 3 h, the mixture was diluted with $CHCl_3$. The organic layer was washed with H_2O and brine, dried (Na_2SO_4), and concentrated. The residue was purified by column chromatography (SiO_2, 10–25% MeOH in $CHCl_3$) to give **2** (3.00 g, 4.82 mmol) in 94% yield: ^{1}H NMR (DMSO-d_6) δ 0.13 (s, 6H), 0.97 (s, 9H), 3.94 (s, 6H), 6.96–7.61 (m, 13H), all additional signals correspond to glycerol and aminobutyl moieties; ^{13}C NMR (DMSO-d_6) δ *−5.6*, 17.7, 25.6, 26.8, 27.8, 48.5, 55.0, 61.7, 62.3, 72.5, 85.2, 113.1, 126.6, 127.6, 127.7, 129.6, 135.5, 144.9, 149.3, 155.8, 158.0; HRMS (FAB) calcd for $C_{35}H_{51}N_2O_6Si$ (MH^+) 623.3516, found 623.3508.

3.1.2. 1-*O*-(4,4′-Dimethoxytrityl)-2-*O*-[*N*-palmitoyl-*N*-(4-aminobutyl)-carbamoyl]-3-*O*-*tert*-butyldimethylsilylglycerol (3)

A mixture of **2** (0.90 g, 1.44 mmol), palmitic acid (0.55 g, 2.16 mmol), and 1-ethyl-3-(3-dimethylaminopropyl)carbodiimide hydrochloride (WSCI) in CH_2Cl_2 (14 mL) was stirred at room

temperature. After 24 h, the mixture was diluted with $CHCl_3$. The organic layer was washed with H_2O and brine, dried (Na_2SO_4), and concentrated. The residue was purified by column chromatography (SiO_2, 10–50% EtOAc in hexane) to give **3** (0.85 g, 0.99 mmol) in 69% yield: ^1H NMR ($CDCl_3$) δ 0.01 (s, 6H), 0.82 (s, 9H), 3.80 (s, 6H), 6.81–7.46 (m, 13H), all additional signals correspond to glycerol, palmitoyl, and aminobutyl moieties; ^{13}C NMR ($CDCl_3$) δ −5.4, 14.1, 18.1, 22.7, 25.7, 26.6, 27.5, 29.3, 29.4, 29.5, 29.6, 29.7, 31.9, 36.7, 39.0, 40.3, 55.1, 60.4, 62.1, 62.4, 74.0, 85.7, 113.0, 126.6, 127.7, 128.1, 130.0, 130.1, 136.0, 136.1, 144.9, 156.2, 158.3, 173.3.

3.1.3. 1-*O*-(4,4′-Dimethoxytrityl)-2-*O*-[*N*-palmitoyl-N-(4-aminobutyl)carbamoyl]glycerol (6)

A mixture of **3** (0.75 g, 0.87 mmol) and TBAF (1 M in THF, 2.00 mL, 2.00 mmol) in THF (4.4 mL) was stirred at room temperature. After 1 h, the mixture was diluted with EtOAc. The organic layer was washed with H_2O and brine, dried (Na_2SO_4), and concentrated. The residue was purified by column chromatography (SiO_2, EtOAc) to give **6** (0.52 g, 0.70 mmol) in 80% yield: ^1H NMR ($CDCl_3$) δ 3.81 (m, 6H), 6.81–7.43 (m, 13H), all additional signals correspond to glycerol, palmitoyl and aminobutyl moieties; ^{13}C NMR ($CDCl_3$) δ 13.8, 14.1, 20.5, 22.7, 25.7, 26.7, 27.2, 29.3, 29.5, 29.6, 29.7, 31.9, 36.8, 39.0, 40.6, 52.1, 55.2, 62.9, 63.2, 74.6, 86.1, 113.1, 126.8, 127.8, 128.0, 130.0, 135.7, 144.6, 156.6, 158.4, 173.4; HRMS (FAB) calcd for $C_{45}H_{67}N_2O_7$ (MH^+) 747.4949, found 747.4955.

3.1.4. 1-*O*-(4,4′-Dimethoxytrityl)-2-*O*-[*N*-oleoyl-N-(4-aminobutyl)carbamoyl]-3-*O*-*tert*-butyldimethylsilylglycerol (4)

A mixture of **2** (1.50 g, 2.41 mmol), oleic acid (1.15 mL, 3.62 mmol), and WSCI in CH_2Cl_2 (12 mL) was stirred at room temperature. After 24 h, the mixture was diluted with $CHCl_3$. The organic layer was washed with H_2O and brine, dried (Na_2SO_4), and concentrated. The residue was purified by column chromatography (SiO_2, 0–5% MeOH in $CHCl_3$) to give **4** (1.83 g, 2.06 mmol) in 86% yield: ^1H NMR ($CDCl_3$) δ 0.04 (s, 6H), 0.85 (s, 9H), 3.82 (s, 6H), 6.84–7.49 (m, 13H), all additional signals correspond to glycerol, oleoyl, and aminobutyl moieties; ^{13}C NMR ($CDCl_3$) δ −5.4, 14.1, 18.1, 22.7, 25.7, 26.6, 27.1, 27.2, 27.5, 29.1, 29.2, 29.3, 29.5, 29.6, 29.7, 29.8, 31.9, 36.7, 39.0, 40.4, 50.6, 55.1, 60.4, 62.2, 62.4, 74.0, 85.8, 113.0, 126.6, 127.7, 128.1, 129.7, 130.0, 130.1, 136.0, 136.1, 144.9, 156.3, 158.4, 173.3; Anal. Calcd for $C_{53}H_{82}N_2O_7Si{\cdot}CHCl_3$: C, 64.43; H, 8.31; N, 2.78. Found: C, 64.32; H, 8.33; N, 2.75.

3.1.5. 1-*O*-(4,4′-Dimethoxytrityl)-2-*O*-[*N*-oleoyl-*N*-(4-aminobutyl)carbamoyl]glycerol (7)

A mixture of **4** (1.66 g, 1.88 mmol) and TBAF (1 M in THF, 3.76 mL, 3.76 mmol) in THF (18 mL) was stirred at room temperature. After 7 h, the mixture was diluted with EtOAc. The organic layer was washed with H_2O and brine, dried (Na_2SO_4), and concentrated. The residue was purified by column chromatography (SiO_2, 0–10% MeOH in $CHCl_3$) to give **7** (1.19 g, 1.54 mmol) in 82% yield: ^1H NMR ($CDCl_3$) δ 3.78 (s, 6H), 6.81–7.43 (m, 13H), all additional signals correspond to glycerol, oleoyl, and aminobutyl moieties; ^{13}C NMR ($CDCl_3$) δ 14.1, 22.6, 25.7, 26.7, 27.1, 29.1, 29.2, 29.4, 29.6, 29.7, 31.8, 32.5, 36.7, 38.9, 40.5, 55.1, 62.8, 63.1, 74.5, 86.1, 113.1, 126.7, 127.8, 128.0, 129.7, 129.9, 135.7, 144.6, 156.6, 158.4, 173.3; Anal. Calcd for $C_{47}H_{68}N_2O_7{\cdot}10/3CHCl_3$: C, 51.63; H, 6.14; N, 2.93. Found: C, 51.79; H, 6.08; N, 2.48.

3.1.6. 1-*O*-(4,4′-Dimethoxytrityl)-2-*O*-[*N*-cholesteryloxycarbonyl-*N*-(4-aminobutyl)carbamoyl]-3-*O*-*tert*-butyldimethylsilylglycerol (5)

A mixture of cholesterol (0.22 g, 0.58 mmol) and *N*,*N*′-carbonyldiimidazole (0.10 g, 0.63 mmol) in pyridine (3 mL) was stirred at room temperature. After 2 h, **2** (0.43 g, 0.70 mmol) was added to the mixture, and the whole was stirred at room temperature. After 12 h, the mixture was diluted with EtOAc. The organic layer was washed with aqueous $NaHCO_3$ (saturated) and brine, dried (Na_2SO_4), and concentrated. The residue was purified by column chromatography (SiO_2, 10% EtOAc in hexane) to give **5** (0.39 g, 0.37 mmol) in 64% yield: ^1H NMR ($CDCl_3$) δ 0.10 (s, 6H), 0.81 (s, 9H), 3.79 (s, 6H), 6.80–7.44 (m, 13H), all additional signals correspond to glycerol, cholesterol, and aminobutyl moieties; ^{13}C NMR ($CDCl_3$) δ −5.4, −3.6, 11.8, 18.0, 18.7, 19.3, 21.0, 22.5, 22.8, 23.8, 24.3, 25.6, 25.8, 27.3, 28.0, 28.1, 28.2, 31.8, 31.9, 35.8, 36.2, 36.5, 37.0, 38.5, 39.5, 39.7, 40.6, 42.3, 50.0, 55.2, 56.1, 56.7, 62.1, 85.8, 113.0, 122.4, 126.6, 127.7, 128.1, 130.0, 136.1, 139.8, 144.9, 156.1, 158.3; Anal. Calcd for $C_{63}H_{94}N_2O_8Si{\cdot}2H_2O$: C, 70.62; H, 9.22; N, 2.61. Found: C, 70.72; H, 9.45; N, 2.43.

3.1.7. 1-*O*-(4,4′-Dimethoxytrityl)-2-*O*-[*N*-cholesteryloxycarbonyl-*N*-(4-aminobutyl)carbamoyl]glycerol (8)

A mixture of **5** (0.34 g, 0.33 mmol) and TBAF (1 M in THF, 1.00 mL, 1.00 mmol) in THF (5 mL) was stirred at room temperature. After 4 h, the mixture was concentrated in vacuo. The residue was purified by column chromatography (SiO_2, 20–100% EtOAc in hexane) to give **8** (0.61 g, 0.18 mmol) in 53% yield: ^1H NMR ($CDCl_3$) δ 3.73 (s, 6 H), 6.75–7.37 (m, 13H), all additional signals correspond to glycerol, cholesterol, and aminobutyl moieties; ^{13}C NMR ($CDCl_3$) δ 11.8, 18.7, 19.3, 21.0, 22.5, 22.8, 23.8, 24.3, 27.1, 27.3, 28.0, 28.1, 28.2, 31.8, 31.9, 35.8, 36.1, 36.5, 36.9, 38.5, 39.5, 39.7, 40.7, 42.3, 49.9, 55.2, 56.1, 56.6, 62.9, 63.4, 74.5, 86.2, 113.1, 122.5, 126.8, 127.8, 128.0, 130.0, 130.1, 135.7, 135.7, 139.8, 144.6, 156.2, 158.5; Anal. Calcd for $C_{57}H_{80}N_2O_8{\cdot}1/3H_2O$: C, 73.83; H, 8.77; N, 3.02. Found: C, 73.87; H, 8.68; N, 2.92.

3.2. Solid support synthesis

A mixture of **6** (0.52 g, 0.70 mmol), succinic anhydride (0.21 g, 2.10 mmol), and DMAP (86 mg, 0.70 mmol) in pyridine (7 mL) was stirred at room temperature. After 24 h, the solution was partitioned between $CHCl_3$ and H_2O, and the organic layer was washed with H_2O and brine. The separated organic phase was dried (Na_2SO_4) and concentrated to give a succinate. Aminopropyl controlled pore glass (0.81 g, 0.18 mmol) was added to a solution of the succinate (0.55 g, 0.61 mmol) and WSCI (0.13 g, 0.70 mmol) in DMF (18 mL), and the mixture was kept for 72 h at room temperature. After the resin was washed with pyridine, a capping solution (20 mL, 0.1 M DMAP in pyridine/Ac_2O = 9:1, v/v) was added and the whole mixture was kept for 24 h at room temperature. The resin was washed with MeOH and acetone, and dried in vacuo. Amount of loaded compound **6** to solid support was 28 μmol/g from calculation of released dimethoxytrityl cation by a solution of 70% $HClO_4$/EtOH (3:2, v/v). In a similar manner, solid supports with **7** and **8** were obtained in 83 and 88 μmol/g loading amounts, respectively.

3.3. RNA synthesis

Synthesis was carried out with a DNA/RNA synthesizer by phosphoramidite method. Deprotection of bases and phosphates was performed in concentrated NH_4OH/EtOH (3:1, v/v) at room temperature for 12 h. 2′-TBDMS groups were removed by 1.0 M tetrabutylammonium fluoride (TBAF, Aldrich) in THF at room temperature for 12 h. The reaction was quenched with 0.1 M TEAA buffer (pH 7.0) and desalted on a Sep-Pak C18 cartridge. Deprotected ONs were purified by 20% PAGE containing 7 M urea to give the highly purified ON**27** (49), ON**28** (24), ON**29** (7), ON**30** (41), ON**31** (19), ON**32** (11), ON**39**(13), ON**40**(8), ON**41**(9), ON**42**(9), ON**43**(11), and ON**44**(6). The yields are indicated in parentheses as OD units at 260 nm starting from 1.0 μmol scale. Extinction coefficients of the

ONs were calculated from those of mononucleotides and dinucleotides according to the nearest-neighbor approximation method.[25]

3.4. MALDI-TOF/MS analyses of RNAs

Spectra were obtained with a time-of-flight mass spectrometer. ON**27**: calculated mass, 7009.5; observed mass, 7003.4. ON**28**: calculated mass, 7035.5; observed mass, 7025.8. ON**29**: calculated mass, 7183.8; observed mass, 7177.2. ON**30**: calculated mass, 7318.8; observed mass, 7311.9. ON**31**: calculated mass, 7344.8; observed mass, 7337.4. ON**32**: calculated mass, 7493.0; observed mass, 7486.3. ON**39**: calculated mass, 7223.7; observed mass, 7220.4. ON**40**: calculated mass, 7074.5; observed mass, 7070.1. ON**41**: calculated mass, 7249.8; observed mass, 7250.2. ON**42**: calculated mass, 7100.6; observed mass, 7099.4. ON**43**: calculated mass, 7398.0; observed mass, 7397.8. ON44: calculated mass, 6530.0; observed mass, 6538.4.

3.5. Dual-luciferase assay

HeLa cells were grown at 37 °C in a humidified atmosphere of 5% CO_2 in air in minimum essential medium (MEM) (Invitrogen) supplemented with 10% fetal bovine serum (FBS). Twenty-four hours before transfection, HeLa cells (4×10^4/mL) were transferred to 96-well plates (100 μL per well). They were transfected, using TransFast (Promega), according to instructions for transfection of adherent cell lines. Cells in each well were transfected with a solution (35 μL) of 20 ng of psiCHECK-2 vector (Promega), the indicated amounts of siRNAs, and 0.3 μg of TransFast in Opti-MEM I Reduced-Serum Medium (Invitrogen), and incubated at 37 °C. After 1 h, MEM (100 μL) containing 10% FBS and antibiotics was added to each well, and the whole was further incubated at 37 °C. After 24 h, cell extracts were prepared in Passive Lysis Buffer (Promega). Activities of firefly and *Renilla* luciferases in cell lysates were determined with a dual-luciferase assay system (Promega) according to the manufacturer's protocol. The results were confirmed by at least three independent transfection experiments with two cultures each and are expressed as the average from four experiments as means ± SD.

3.6. Cell culture and transfection

HT-1080 human fibrosarcoma (HT-1080) cells were cultured in RPMI 1640 supplemented with streptomycin (0.1 mg/mL), penicillin (100 U/mL), and 10% heat-inactivated fetal bovine serum. Cells were cultured at 37 °C with a 5% CO_2 atmosphere. Cells were seeded in 35-mm dishes at density of 120,000 cells per dish and allowed to attach to the culture vessel for 24 h prior to transfection. Transfection solutions were prepared according to the manufacturer's protocols with an antibiotic-free medium. siRNA was diluted in 250 μL of RPMI 1640 without antibiotics and serum. Five micrograms of Lipofectamine 2000 (Invitrogen) was diluted in 250 μl of RPMI 1640 without antibiotics and serum. After 5 min of incubation, they were combined and incubated for 20 min at room temperature to form the siRNA-lipid complexes. Five hundred microliters of the transfection solution was dispensed per dish. Transfections were conducted for 6 h, after which the solution was removed and replaced with growth medium containing antibiotics. Cells were harvested for each analysis 24 or 48 h post-transfection.

3.7. Western blot analysis for human RNase L

HT-1080 cells were harvested by washing the cells once with 1× PBS, aspirated, and treated with 1 mL of a trypsin solution at 37 °C for 1 min. Trypsin was inactivated by the addition of a culture medium containing 10% FBS. The contents of each dish were transferred separately into 1.5 mL microfuge tubes and centrifuged at 2500 rpm for 5 min at 4 °C. The supernatant fluid was discarded, and the cell pellet was resuspended in 2 volumes of hypotonic buffer A (0.5% (v/v) Nonidet P-40, 20 mM Hepes, pH 7.5, 10 mM KOAc, 15 mM $Mg(OAc)_2$, 1 mM dithiothreitol, 1 mM phenylmethylsulfonyl fluoride, 10 μg/mL aprotinin) and allowed to swell in this buffer for 10 min before being broken either by 30 strokes in a tight-fitting glass Dounce homogenizer for 2 min in ice. The homogenate was centrifuged at 10,000g for 10 min and the supernatant was pipetted off and stored at −80 °C. Cell extracts were separated by 7.5% SDS–PAGE. The proteins were electrophoretically transferred to PVDF membrane. Primary antibodies, mouse monoclonal anti-human RNase L antibody, that were obtained from Taiho Pharmaceutical Co., Ltd, were diluted 1:5600 in TTBS containing 5% BSA and placed on a rocker platform for 16 h at 4 °C. The membranes were washed once for 15 min and then three times for 5 min each in TTBST. Secondary antibody conjugate (HRP conjugated anti-mouse IgG) was diluted 1:100,000 in TTBS containing 5% BSA and placed on a rocker platform for 16 h at 25 °C. The membranes were washed once for 15 min and then three times for 5 min each in TTBST. Immunoreactive bands were detected by enhanced chemiluminescence (utilizing ECL plus chemiluminescence detection reagents from Amersham) and subsequent exposure to X-ray film.

Acknowledgments

This work was supported by a Grant from PRESTO of the Japan Science and Technology Agency (JST) and a Grant-in-Aid for Scientific Research from the Japan Society for the Promotion of Science (JSPS). We are grateful to Professor Y. Tomari (the University of Tokyo) for helpful discussions. We are also grateful to Professor Y. Hirata (Gifu University) and Professor K. Kiuchi (Gifu University) for providing technical assistance in the dual-luciferase assay.

References

1. Fire, A.; Xu, S.; Montgomery, M. K.; Kostas, S. A.; Driver, S. E.; Mello, C. C. *Nature* **1998**, *391*, 806.
2. Bumcrot, D.; Manoharan, M.; Koteliansky, V.; Sah, D. W. Y. *Nat. Chem. Biol.* **2006**, *2*, 711.
3. Song, E.; Lee, S.-K.; Wang, J.; Ince, N.; Ouyang, N.; Min, J.; Chen, J.; Shankar, P.; Lieberman, J. *Nat. Med.* **2003**, *3*, 347.
4. Soutschek, J.; Akinc, A.; Bramlage, B.; Charisse, K.; Constien, R.; Donoghue, M.; Elbashir, S.; Geick, A.; Hadwiger, P.; Harborth, J.; John, M.; Kesavan, V.; Lavin, G.; Pandey, R. K.; Racie, T.; Rajeev, K. G.; Röhl, I.; Toudjarska, I.; Wang, G.; Wuschko, S.; Bumcrot, D.; Koteliansky, V.; Limmer, S.; Manoharan, M.; Vornlocher, H.-P. *Nature* **2004**, *432*, 173.
5. Wolfrum, C.; Shi, S.; Jayaprakash, K. N.; Jayaraman, M.; Wang, G.; Pandey, R. K.; Rajeev, K. G.; Nakayama, T.; Charrise, K.; Ndungo, E. M.; Zimmermann, T.; Koteliansky, V.; Manoharan, M.; Stoffel, M. *Nat. Biotech.* **2007**, *25*, 1149.
6. Minakuchi, Y.; Takeshita, F.; Kosaka, N.; Sasaki, H.; Yamamoto, Y.; Kouno, M.; Honma, K.; Nagahara, S.; Hanai, K.; Sano, A.; Kato, T.; Terada, M.; Ochiya, T. *Nucleic Acids Res.* **2004**, *32*, e109.
7. Song, E.; Zhu, P.; Lee, S.-K.; Chowdhury, D.; Kussman, S.; Dykxhoorn, D. M.; Feng, Y.; Palliser, D.; Weiner, D. B.; Shankar, P.; Marasco, W. A.; Lieberman, J. *Nat. Biotech.* **2005**, *23*, 709.
8. Morrissey, D. V.; Lockridge, J. A.; Shaw, L.; Blanchard, K.; Jensen, K.; Breen, W.; Hartsough, K.; Machemer, L.; Radka, S.; Jadhav, V.; Vaish, N.; Zinnen, S.; Vargeese, C.; Bowman, K.; Shaffer, C. S.; Jeffs, L. B.; Judge, A.; MacLachlan, I.; Polisky, B. *Nat. Biotech.* **2005**, *23*, 1002.
9. McNamara, J. O., II; Andrechek, E. R.; Wang, Y.; Viles, K. D.; Rempel, R. E.; Gilboa, E.; Sullenger, B. A.; Giangrande, P. H. *Nat. Biotech.* **2006**, *24*, 1005.
10. Tolia, N. H.; Joshua-Tor, L. *Nat. Chem. Biol.* **2007**, *3*, 36.
11. Parker, J. S.; Roe, S. M.; Barford, D. *Nature* **2005**, *434*, 663.
12. Ma, J.-B.; Yuan, Y.-R.; Meister, G.; Pei, Y.; Tuschl, T.; Patel, D. J. *Nature* **2005**, *434*, 666.
13. Nykänen, A.; Haley, B.; Zamore, P. D. *Cell* **2001**, *107*, 309.
14. Schwarz, D. S.; Hutvágner, G.; Haley, B.; Zamore, P. D. *Mol. Cell* **2002**, *10*, 537.
15. Lingel, A.; Simon, B.; Izaurralde, E.; Sattler, M. *Nature* **2003**, *426*, 465.
16. Yan, K. S.; Yan, S.; Farooq, A.; Han, A.; Zeng, L.; Zhou, M.-M. *Nature* **2003**, *426*, 469.

17. Song, J.-J.; Liu, J.; Tolia, N. H.; Schneiderman, J.; Smith, S. K.; Martienssen, R. A.; Hannon, G. J.; Joshua-Tor, L. *Nat. Struct. Biol.* **2003**, *12*, 1026.
18. Ma, J. B.; Te, K.; Patel, D. J. *Nature* **2004**, *429*, 318.
19. Elbashir, S. M.; Martinez, J.; Patkaniowska, A.; Lendeckel, W.; Tuschl, T. *EMBO J.* **2001**, *20*, 6877.
20. De Napoli, L.; Di Fabio, G.; Messere, A.; Montesarchio, D.; Musumeci, D.; Piccialli, G. *Tetrahedron* **1999**, *55*, 9899.
21. Mammond, S. M.; Boettcher, S.; Caudy, A. A.; Kobayashi, R.; Hannon, G. J. *Science* **2001**, *293*, 1146.
22. Martinez, J.; Patkaniowska, A.; Urlaub, H.; Lührmann, R.; Tuschl, T. *Cell* **2002**, *110*, 563.
23. Hassel, B. A.; Zhou, A.; Sotomayor, C.; Maran, A.; Silverman, R. H. *EMBO J.* **1993**, *12*, 3297.
24. Zhou, A.; Paranjape, J.; Brown, T. L.; Nie, H.; Naik, S.; Dong, B.; Chang, A.; Trapp, B.; Fairchild, R.; Colmenares, C.; Silverman, R. H. *EMBO J.* **1997**, *16*, 6355.
25. Puglisi, J. D.; Tinoco, I., Jr.. In *Methods in Enzymology*; Dahlberg, J. E., Abelson, J. N., Eds.; Academic Press, Inc.: San Diego, 1989; Vol. 180, pp 304–325.

Genomics 92 (2008) 9–17

Contents lists available at ScienceDirect

Genomics

journal homepage: www.elsevier.com/locate/ygeno

Gene expression profiles of necrosis and apoptosis induced by 5-fluoro-2′-deoxyuridine

Akira Sato [a], Akiko Hiramoto [a], Yusuke Uchikubo [a], Eriko Miyazaki [a], Akito Satake [a], Tomoharu Naito [a], Osamu Hiraoka [b], Tsuyoshi Miyake [c], Hye-Sook Kim [a], Yusuke Wataya [a,*]

[a] Faculty of Pharmaceutical Sciences, Okayama University, Tsushima, Okayama 700-8530, Japan
[b] School of Pharmacy, Shujitsu University, Nishigawara, Okayama 703-8516, Japan
[c] Department of Chemical Technology, Industrial Technology Center of Okayama Prefecture, 5301, Haga, Okayama 701-1296, Japan

ARTICLE INFO

Article history:
Received 23 October 2007
Accepted 8 February 2008

Keywords:
5-Fluoro-2′-deoxyuridine
Microarray analysis
Gene expression profile
Cell death
Necrosis
Apoptosis

ABSTRACT

5-Fluoro-2′-deoxyuridine (FUdR), a potent anticancer agent, exerts its effects by inhibiting thymidylate synthase, an essential machinery for DNA synthesis in cell proliferation. Also, cell death is caused by FUdR, primarily due to an imbalance in the nucleotide pool resulting from this enzyme inhibition. We have investigated the cancer cell death induced by FUdR, focusing on its molecular mechanisms. Using mouse mammary tumor FM3A cell lines, the original clone F28-7 and its variant F28-7-A cells, we previously reported an interesting observation that FUdR induces a necrotic morphology in F28-7, but induces, in contrast, an apoptotic morphology in F28-7-A cells. In the present study, to understand the molecular mechanisms underlying these differential cell deaths, i.e., necrosis and apoptosis, we investigated the gene expression changes occurring in these processes. Using the cDNA microarray technology, we found 215 genes being expressed differentially in the necrosis and apoptosis. Further analysis revealed differences between these cell lines in terms of the expressions of both a cluster of heat shock protein (HSP)-related genes and a cluster of apoptosis-related genes. Notably, inhibition of HSP90 in F28-7 cells caused a shift from the FUdR-induced necrosis into apoptosis. These findings are expected to lead to a better understanding of this anticancer drug FUdR for its molecular mechanisms and also of the general biological issue, necrosis and apoptosis.

Introduction

5-Fluoro-2′-deoxyuridine (FUdR), a potent anticancer agent, exerts its effects by inhibiting thymidylate synthase, an essential machinery for DNA synthesis in cell proliferation [1–6]. 5-Fluoro-2′-deoxyuridine 5′-monophosphate has been shown to form a covalent complex with thymidylate synthase in the presence of 5,10-methylenetetrahydrofolate [3–6]. The inhibition of thymidylate synthesis causes an imbalance in the deoxyribonucleoside triphosphate (dNTP) pool, leading to cell death [7].

Although cell death is, on one hand, associated with normal cellular development and homeostasis, it is associated with various pathological processes. Two general pathways for cell death have been defined, apoptosis and necrosis. Depending on the cell type, cellular context, or stimulus, a cell may die by apoptosis or by necrosis [8]. Apoptosis is morphologically characterized by membrane blebbing, shrinking of the cell and its organelles, and oligonucleosomal degradation of DNA, followed by disintegration of the cell; and the resulting fragments are phagocytosed by neighboring cells [9,10]. In contrast, necrosis is characterized by swelling of the cell and the organelles, and the disruption of the cell membrane, resulting in cell lysis. Necrosis is often accompanied by inflammation due to release of the cellular components [8,11]. The molecular mechanisms of apoptosis have been well studied, whereas less is known about the processes involved in necrosis. In recent years, research on necrosis and apoptosis has attracted much attention, because disruption of cell death pathways can lead to various diseases.

We have investigated the molecular mechanisms regulating necrosis and apoptosis that occur on treatment of mouse mammary tumor FM3A cells with FUdR, using the original clone F28-7 and its variant F28-7-A cells. Previously, we reported that the treatment can induce in F28-7 cells a breakdown of DNA into chromosome-sized fragments leading to necrosis; on the other hand, it can induce in F28-7-A a more extensive DNA cleavage into oligonucleosome-sized fragments and subsequent development of apoptosis [12]. These observations prompted us to further investigate the cytotoxic action of FUdR, with the hope to better understand the molecular mechanisms of the activities of this drug and also to obtain clues for the elucidation of general biological phenomena, necrosis and apoptosis. Recent development of genomics has now enabled us for the first time analyze the gene expression profiles of necrosis induced by FUdR in F28-7 cells and those of apoptosis in F28-7-A cells. Using cDNA microarray technology, the study revealed 215 genes that were differentially expressed in the FUdR-induced necrosis and apoptosis. Of particular interest were changes in the expression pattern

* Corresponding author. Fax:+81 86 251 7974.
E-mail address: wataya@cc.okayama-u.ac.jp (Y. Wataya).

0888-7543/$ – see front matter © 2008 Elsevier Inc. All rights reserved.
doi:10.1016/j.ygeno.2008.02.002

of a group of apoptosis-related genes, including BCL-2 family members and caspases, a family of cysteine proteases. Another interesting group was the heat shock protein (HSP) family and related genes, including DnaJ (Hsp40) homolog, subfamily B, member 4 (*Dnajb4*), heat shock protein 110 (*Hsp110*), and AHA1, activator of heat shock protein ATPase homolog 1 (*Ahsa1*). An immunofluorescence study revealed that FUdR can induce release of cytochrome *c* from mitochondria to the cytoplasm and nucleus in F28-7-A cells, but not in F28-7 cells. However, a combined treatment with FUdR and geldanamycin (GA), the latter being an inhibitor toward a molecular chaperone HSP90, caused DNA cleavage into oligonucleosome-size fragments, an apoptotic morphology, followed by release of cytochrome *c* from mitochondria to cytoplasm and to nucleus in F28-7 cells. These findings suggest that HSP90 can play an important role in the regulation of cell death. It should be noted that the involvement of HSP90 has been recognized as being associated with various cell activities, e.g., cell cycle control, cell development, and cell death [13–19].

Results

Gene expression profiles in FUdR-induced necrosis and apoptosis

To profile the changes in the pattern of gene expression in FUdR-induced necrosis and apoptosis, F28-7 and F28-7-A cells were treated with 1 μM FUdR for 0 (no drug, no incubation), 4, 8, and 16 h. The treatment with FUdR caused induction of necrosis in F28-7 cells and apoptosis in F28-7-A cells. In agreement with our previous report [12], both F28-7 and F28-7-A exhibited a very similar cell morphology in the absence of FUdR (both at 0 time and at 16 h; data not shown). The treatment periods we chose for the analysis of this drug action were based on our previous studies [12]: namely, at 4 h no decrease in viability; at 8 h still no decrease in viability; at 16 h significant decrease notable, about 60% with F28-7, and about 80% with F28-7-A. At each time period, cells were collected and the total RNA was isolated and reverse-transcribed, and the cDNAs produced were subjected to microarray analysis. For both of these cells at each time of the treatment, three independent analyses were performed with the GeneChip Mouse Expression Array 430A, which contains 22,600 probe sets and can be used to analyze the expression level of ~14,000 known mouse genes.

For statistical analysis, the one-way analysis of variance (ANOVA) was performed on all the genes of the probe sets, and a change in gene expression was considered significant if the *P* value was less than 0.001 after application of the Bonferroni correction. Thus, 411 probe sets representing 371 genes were identified as differentially expressed in F28-7 and F28-7-A cells at each time period of the treatment (including the 0 h). The selected genes were then classified by hierarchical clustering according to the similarity in their expression profile, and as a result five clusters were generated as shown in Fig. 1. As can be seen in this figure, the gene expression-change patterns differed considerably between F28-7 and F28-7-A during the course of the treatment. These changes obviously deserved extensive investigation.

A remarkable observation was that in the untreated stage (the 0 h samples), 113 genes are differentially expressed (more than +/− 1.5-fold) in F28-7 and F28-7-A cells. These differentially expressed genes were grouped by their function, apoptosis, cytoskeleton organization, signal transduction, transcription, and transport. In these 113 genes, 29 genes were expressed with a large difference (more than 10-fold). They are listed in Supplementary Data (Supplementary Table 1). On the other hand, the expression of 18 genes changed dynamically (more than 10-fold) during the FUdR treatment in either F28-7 or F28-7-A cells. Among them, the changes in 3 genes had a similar pattern in F28-7 and F28-7-A cells. Therefore, there were 15 genes that had a greatly different manner of change between the necrosis and apoptosis. We suspect that these genes include those that determine the death pattern. These 15 genes are listed in Supplementary Data (Supplementary Table 2).

Gene clusters 1 and 3 are those differentially expressed in necrosis and apoptosis in the FUdR treatment. Cluster 3 contained genes with upregulated expressions and cluster 1 those with downregulated expressions in the induced necrosis as compared to the apoptosis. Genes in clusters 2, 4, and 5 were expressed similarly in both types of cell death. These gene lists are provided as Supplementary Data (Supplementary Tables 3 to 5).

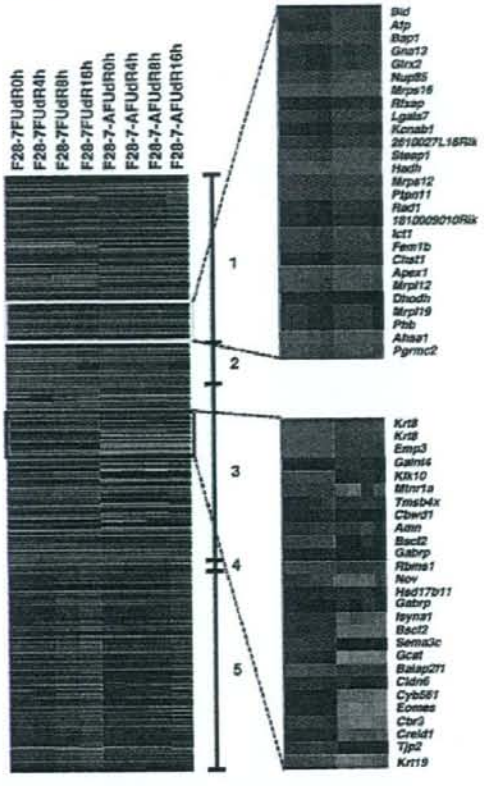

Fig. 1. Gene expression profiles in F28-7 and F28-7-A cells treated with FUdR. RNA isolated from FM3A cells F28-7 and F28-7-A that had been treated with 1 μM FUdR for 0 (no drug, no incubation), 4, 8, or 16 h was subjected to microarray analysis using GeneChip Mouse Expression Array 430 A (Affymetrix). For each cell line, three independent experiments were performed at individual treatment times. Gene expression data were analyzed using Array Assist ver. 5.2. software (Stratagene). For statistical analysis, 411 probe sets were selected as differentially expressed genes in apoptosis and necrosis after treatment with FUdR, using ANOVA with the *P* values set at smaller than 0.001. Then, the selected genes were subjected to hierarchical clustering. Numbers 1–5 indicate five different clusters identified by hierarchical clustering. The yellow and blue boxes indicate genes of cluster 1 and cluster 3, respectively. Higher signal values are shown in red, and lower signal values in green.

Differentially expressed genes in necrosis and apoptosis were grouped by their functions, and catalogued in Table 1 (cluster 3) and Table 2 (cluster 1). These functions include apoptosis, cell adhesion, cell cycle, cell growth, cell motility, cell proliferation and differentiation, development, DNA repair and replication, chromatin modification, cytoskeleton organization, keratinisation, plasma membrane repair, immune response, redox homeostasis, metabolism, mRNA processing, ATP biosynthesis, phospholipid biosynthesis, fatty acid biosynthesis, protein synthesis and folding, protein modification and degradation, signal transduction, transcription, and transport (Tables 1 and 2). These differentially expressed genes are those functioning at various stages of important biological processes. In particular, genes corresponding to a number of apoptosis regulators were shown to exhibit the differential expressions. These genes included B-cell leukemia/lymphoma 10 (*Bcl10*), BH3 interacting domain death agonist (*Bid*), caspase-1 (*Casp1*), death-associated protein (*Dap*),

Table 1
Functional categorization of upregulated genes in necrosis (total: 104 genes)

GenBank	Gene title
Apoptosis	
BG071931	calcium/calmodulin-dependent protein kinase ID ***(Camk1d)***
NM_130859.1	caspase recruitment domain family, member 10 ***(Card10)***
AF047838.1	***chloride channel calcium activated 1 (Clca1)***
BC021786.1	integral membrane protein 2B ***(Itm2b)***
NM_011111.1	***serine (or cysteine) peptidase inhibitor, clade B,member 2 (Serpinb2)***
Cell adhesion	
BC005718.1	claudin 6 ***(Cldn6)***
BB132473	L1 cell adhesion molecule ***(L1cam)***
NM_011345.1	***selectin, endothelial cell (Sele)***
Cell cycle	
AV126179	***centrosomal protein 55 (Cep55)***
Cell growth	
BC001999.1	epithelial membrane protein 3 ***(Emp3)***
X96585.1	***nephroblastoma overexpressed gene (Nov)***
Cell motility	
AK017725.1	***tropomodulin 3 (Tomod3)***
Development	
NM_033603.1	***amnionless (Amn)***
AK003744.1	cystatin E/M ***(Cst6)***
D85028.2	sema domain, immunoglobulin domain (Ig), basic domain, secreted, (semaphorin) 3A ***(Sema3a)***
NM_013657.1	***sema domain, immunoglobulin domain (Ig), basic domain, secreted, (semaphorin) 3C (Sema3c)***
DNA repair and DNA replication	
NM_007948.1	***excision repair cross-complementing rodent repair deficiency, complementation group 1 (Ercc1)***
BC002257.1	RIKEN cDNA 2610305J24 gene ***(2610305J24Rik)***
NM_020296.1	***RNA binding motif, single stranded interacting protein 1 (Rbms1)***
Chromatin modification	
NM_008197.1	***H1 histone family, member 0 (H1f0)***
NM_011061.1	peptidyl arginine deiminase, type IV ***(Padi4)***
Cytoskeleton organization	
M21836.1	keratin 8 ***(Krt8)***
NM_008471.1	***keratin 19 (Krt19)***
NM_021278.1	***thymosin, beta 4, X chromosome (Tmsb4x)***
Keratinization	
AF126834.1	periplakin ***(Ppl)***
Plasma membrane repair	
BI555209	dysferlin ***(Dysf)***
Immune response	
BC019961.1	***chemokine (C-X-C motif) ligand 16 (Cxcl16)***
NM_010406.1	hemolytic complement ***(Hc)***
Redox homeostasis	
NM_029571.1	KTI12 homolog, chromatin associated (S. cerevisiae) ***(Kti12)***
Metabolism	
NM_019811.1	acyl-CoA synthetase short-chain family member 2***(Acss2)***
BC024934.1	aspartoacylase (aminoacylase) 2 ***(Aspa)***
NM_013847.1	glycine C-acetyltransferase ***(Gcat)***
AA792094	glutamate oxaloacetate transaminase 1, soluble***(Got1)***
NM_008182.1	glutathione S-transferase, alpha 1 (Ya), alpha 2 (Yc2) ***(Gsta2)***
C78422	***coenzyme Q3 homolog, methyltransferase (yeast) (Coq3)***
AK003232.1	***carbonyl reductase 3 (Cbr3)***
BB546344	hydroxysteroid (17-beta) dehydrogenase 11 ***(Hsd17b11)***
NM_009214.1	***spermine synthase (Sms)***
mRNA processing	
BG972112	***RIKEN cDNA 5730453I16 gene (5730453I16Rik)***
ATP biosynthesis	
BG794445	ATP synthase, H+ transporting, mitochondrial F0 complex, subunit f, isoform 2 ***(Atp5j2)***

Table 1 *(continued)*

GenBank	Gene title
Phospholipid biosynthesis	
NM_023627.1	***myo-inositol 1-phosphate synthase A1 (Isyna1)***
Fatty acid biosynthesis	
BB430611	***fatty acid desaturase 2 (Fads2)***
Protein biosynthesis	
NM_025936.1	***arginyl-tRNA synthetase (Rars)***
AF321126.1	eukaryotic translation elongation factor 1 gamma ***(Eef1g)***
BC024463.1	eukaryotic translation initiation factor 3, subunit 6 interacting protein ***(Eif3s6ip)***
BI104847	***eukaryotic translation initiation factor 5 (Eif5)***
NM_007990.1	Finkel-Biskis-Reilly murine sarcoma virus(FBR-MuSV) ubiquitously expressed (fox derived) ***(Fau)***
AV370731	***UDP-N-acetyl-alpha-D-galactosamine:polypeptide N-acetylgalactosaminyltransferase 4 (Galnt4)***
Protein folding	
BI499717	***heat shock protein 110 (Hsp110)***
Protein modification	
NM_018784.1	***ST3 beta-galactoside alpha-2,3-sialyltransferase 6 (St3gal6)***
NM_031386.1	***testis expressed gene 14 (Tex14)***
AV171029	ubiquilin 2 ***(Ubqln2)***
Protein degradation	
NM_008906.1	***cathepsin A (Ctsa)***
NM_133712.1	***kallikrein related-peptidase 10 (Klk10)***
BB250811	***procollagen C-endopeptidase enhancer protein (Pcolce)***
AF334269.1	***WAP four-disulfide core domain 2 (Wfdc2)***
Signal transduction	
BE570050	***AHNAK nucleoprotein (desmoyokin) (Ahnak)***
AK008203.1	BAI1-associated protein 2-like 1 ***(Baiap2l1)***
AV375176	***centaurin, delta 1 (Centd1)***
NM_007974.1	coagulation factor II (thrombin) receptor-like 1 ***(F2rl1)***
BB251922	***cyclic nucleotide phosphodiesterase 1 (Cnp1)***
BB324823	***latent transforming growth factor beta binding protein 3 (Ltbp3)***
NM_008639.1	melatonin receptor 1A ***(Mtnr1a)***
BC024684.1	mitogen-activated protein kinase 6 ***(Mapk6)***
BC011193.1	***prostaglandin E receptor 4 (subtype EP4) (Ptger4)***
Transcription	
BC019946.1	***activating transcription factor 3 (Atf3)***
BC006628.1	centromere protein B ***(Cenpb)***
NM_007913.1	***early growth response 1 (Egr1)***
AB031037.1	***eomesodermin homolog (Xenopus laevis) (Eomes)***
NM_008046.1	***follistatin (Fst)***
NM_010235.1	***fos-like antigen 1 (Fosl1)***
NM_016861.1	***PDZ and LIM domain 1 (elfin) (Pdlim1)***
AU019880	Predicted gene, EG668701 ***(EG668701)***
Transport	
AK005223.1	***adaptor-related protein complex 1, sigma 2 subunit (Ap1s2)***
BC027319.1	ATPase, Na+/K+ transporting, beta 1 polypeptide ***(Atp1b1)***
NM_025911.1	coiled-coil domain containing 91 ***(Ccdc91)***
BC006732.1	***cytochrome b-561 (Cyb561)***
AV007132	frataxin ***(Fxn)***
BC025550.1	gamma-aminobutyric acid (GABA-A) receptor ,pi ***(Gabrp)***
BC024375.1	***growth hormone receptor (Ghr)***
NM_007515.1	solute carrier family 7 (cationic amino acid transporter, y+ system) member 3 ***(Slc7a3)***
AK004616.1	solute carrier organic anion transporter family, member 2a1 ***(Slco2a1)***
Unknown	
AK008203.1	BAI1-associated protein 2-like 1 ***(Baiap2l1)***
BB223872	***Bernardinelli-Seip congenital lipodystrophy 2 homolog (human) (Bscl2)***
BC027558.1	bolA-like 1 (E. coli) ***(Bola1)***
NM_007594.1	calumenin ***(Calu)***
BC018472.1	COBW domain containing 1 ***(Cbwd1)***
NM_133930.1	cysteine-rich with EGF-like domains 1 ***(Creld1)***
BG794917	expressed sequence AI462493 ***(AI462493)***
AK013203.1	***fibronectin type III domain containing 4 (Fndc4)***

(continued on next page)

Table 1 (continued)

GenBank	Gene title
Unknown	
BI080136	***heterogeneous nuclear ribonucleoprotein U-like 2 (Hnrpul2)***
NM_010807.1	***MARCKS-like 1 (Marcksl1)***
AV366860	membrane bound O-acyltransferase domain containing 1 ***(Mboat1)***
NM_022018.1	niban protein ***(Niban)***
AJ647775	***Nur77 downstream gene 2 (Ndg2)***
X96606.1	***ovary testis transcribed (Ott)***
BG065719	***predicted gene,(EG665081)***
BC022950.1	***RIKEN cDNA 1600029D21 gene (1600029D21Rik)***
BI415578	RIKEN cDNA 2210016F16 gene ***(2210016F16Rik)***
NM_133929.1	RIKEN cDNA E330009J07 gene ***(E330009J07Rik)***
BB493265	***small nucleolar RNA, C/D box 22 (Snord22)***
NM_011430.1	synuclein, gamma ***(Sncg)***
BB758095	***tight junction protein 2 (Tjp2)***
AA124553	***zinc finger, AN1-type domain 5 (Zfand5)***

Note: These genes were assigned to cluster 3. Genes showing upregulated expression in necrosis are grouped according to function, and gene symbols are indicated in parentheses. The bold italic-lettered genes were those upregulated > 1.5-fold ($p < 0.001$) in F28-7 cells compared with those in F28-7-A after treatment with FUdR for 16 h.

glutaredoxin 2 (*Glrx2*), lectin, galactose binding, soluble 7 (*Lgals7*), calcium/calmodulin-dependent protein kinase ID (*Camk1d*), caspase recruitment domain family member 10 (*Card10*), chloride channel calcium activated 1 (*Clca1*), integral membrane protein 2B (*Itm2b*), and serine (or cysteine) peptidase inhibitor, clade B, member 2 (*Serpinb2*), with all of the above being involved in a variety of apoptosis signaling. Interestingly, the differentially expressed genes were also associated with the HSP90 chaperone complex including *Hsp110*, *Dnajb4*, and *Ahsa1*. The FUdR-induced expression patterns of apoptosis-related genes, HSP family and related genes, are shown in Supplementary Data (Supplementary Fig. 1 and Fig. 2).

The genes that are related to cell growth, cytoskeleton organization, keratinization, plasma membrane repair, mRNA processing, ATP biosynthesis, phospholipid biosynthesis, and fatty acid biosynthesis were upregulated by the FUdR-induced necrosis. In particular, the nephroblastoma overexpressed gene (*Nov*), keratin 19 (*Krt19*), thymosin, beta 4, X chromosome (*Tmsb4x*), RIKEN cDNA 5730453I16 gene (*5730453I16Rik*), myo-inositol 1-phosphate synthase A1 (*Isya1*), and fatty acid desaturase 2 (*Fads2*) were upregulated more than 1.5-fold in F28-7 cells compared with those in F28-7-A in the treatment with FUdR. Also, some transcription and cell adhesion-related genes, such as activating transcription factor 3 (*Atf3*), early growth response 1 (*Egr1*), and selectin, endothelial cell (*Sele*), had drastic changes in F28-7 cells during FUdR treatment. The expression patterns of *Nov*, *Krt19*, *Tmsb4x*, *Atf3*, *Egr1*, and *Sele* are given in Supplementary Data (Supplementary Fig. 3). The vast majority of these genes have not been previously reported to be affected by FUdR. It should be noted that although the genes for thymidylate synthase (the drug's target) [20], uracil-DNA glycosylase [21], and thymidine kinase [21] were reported to have significant changes in response to FUdR, our microarray analysis had no changes.

As a follow-up to the microarray, we analyzed the mRNA and protein expression levels of the identified apoptosis-related genes, such as *Serpinb2* and *Bid*, using quantitative real-time PCR (Q-PCR) and Western blotting. The mRNA expression levels of *Serpinb2* and protein expression levels of BID are listed in Supplementary Data (Supplementary Figs. 4a and b). The expression patterns of *Serpinb2* and BID in Q-PCR and Western blotting conform with the results of microarray analysis (see Supplementary Fig. 1). We examined in 1998 the time course of mRNA expressions of the *Jun* (*c-jun*), *Fos* (*c-fos*), and *Myc* (*c-myc*) by Northern blot analysis. In these data, the expression patterns of *Jun*, *Fos*, and *Myc* mRNA showed clear upregulations from 8 to 16 h in F28-7 cells. In contrast, little upregulation was observed in F28-7-A [12]. The upregulations of *Jun* and *Fos* mRNA detected in the present experiments with the microarray technique agree with the results of the 1998 Northern blot data. It is common knowledge that the microarray technique is inferior to the

Table 2
Functional categorization of downregulated genes in necrosis (total: 111 genes)

GenBank	Gene title
Apoptosis	
NM_009740.1	B-cell leukemia/lymphoma 10 ***(Bcl10)***
NM_007544.1	***BH3 interacting domain death agonist (Bid)***
BC008152.1	caspase 1 ***(Casp1)***
BC024876.1	***death-associated protein (Dap)***
BB172698	***glutaredoxin 2 (thioltransferase) (Glrx2)***
BC011507.1	***lectin, galactose binding, soluble 7 (Lgals7)***
Cell adhesion	
NM_010581.1	***CD47 antigen (Cd47)***
NM_010494.1	***intercellular adhesion molecule 2 (Icam2)***
AA516617	plakophilin 2 ***(Pkp2)***
AV026492	thrombospondin 1 ***(Thbs1)***
Cell cycle	
BC027022.1	RIKEN cDNA 1810009O10 gene ***(1810009O10Rik)***
AB040489.1	RIKEN cDNA 2610204L23 gene ***(2610204L23Rik)***
Cell motility	
BC002136.1	coronin, actin binding protein 1A ***(Coro1a)***
Cell proliferation and differentiation	
NM_010216.1	***c-fos induced growth factor (Figf)***
BB000455	granulin ***(Grn)***
Development	
BC003916.1	RIKEN cDNA 0610007P06 gene ***(0610007P06Rik)***
NM_011340.1	***serine (or cysteine) peptidase inhibitor, clade F, member 1 (Serpinf1)***
DNA repair and DNA replication	
NM_009687.1	apurinic/apyrimidinic endonuclease 1 ***(Apex1)***
AF072521.1	poly (ADP-ribose) polymerase family, member 2 ***(Parp2)***
AK010619.1	prohibitin ***(Phb)***
NM_011232.1	RAD1 homolog (S. pombe) ***(Rad1)***
Chromatin modification	
U97675.1	embryonic ectoderm development ***(Eed)***
Immune response	
AF316999.1	***DNA segment, Chr 11, Lothar Hennighausen 2, (Picalm) expressed (D11Lgp2e)***
NM_010189.1	***Fc receptor, IgG, alpha chain transporter (Fcgrt)***
BC010229.1	***guanylate binding protein 6 (Gbp6)***
NM_010259.1	***guanylate nucleotide binding protein 1 (Gbp1)***
NM_010260.1	***guanylate nucleotide binding protein 2 (Gbp2)***
NM_008326.1	immunity-related GTPase family, M ***(Irgm)***
NM_008360.1	***interleukin 18 (Il18)***
NM_008787.1	nucleoporin 85 ***(Nup85)***
Redox homeostasis	
NM_025559.1	RIKEN cDNA 1810046J19 gene ***(1810046J19Rik)***
Metabolism	
AK002555.1	***acetyl-Coenzyme A acyltransferase 2 (Acaa2)***
NM_007382.1	***acyl-Coenzyme A dehydrogenase, medium chain (Acadm)***
NM_007398.1	***adenosine deaminase (Ada)***
NM_011996.1	***alcohol dehydrogenase 4 (class II), pi polypeptide (Adh4)***
AF177041.1	***aldo-keto reductase family 1, member C12 (Akr1c12)***
NM_013778.1	***aldo-keto reductase family 1, member C13 (Akr1c13)***
AV124668	alpha fetoprotein ***(Afp)***
D85596.1	***AMP deaminase 3 (Ampd3)***
NM_023850.1	***carbohydrate (keratan sulfate Gal-6) sulfotransferase 1 (Chst1)***
NM_026819.1	dehydrogenase/reductase (SDR family) member 1 ***(Dhrs1)***
NM_020046.1	dihydroorotate dehydrogenase ***(Dhodh)***
BC027422.1	emopamil binding protein-like ***(Ebpl)***
NM_016772.1	***enoyl coenzyme A hydratase 1, peroxisomal (Ech1)***
BC069933	***expressed sequence C80008 (C80008)***
AV307219	galactose mutarotase ***(Galm)***
AK002661.1	glutathione S-transferase kappa 1 ***(Gstk1)***
NM_010357.1	***glutathione S-transferase, alpha 4 (Gsta4)***
AV018774	***hydroxyacyl-Coenzyme A dehydrogenase (Hadh)***
BM200015	hydroxysteroid dehydrogenase like 2 ***(Hsdl2)***
AK009478.1	***peroxisomal delta3, delta2-enoyl-Coenzyme A isomerase (Peci)***
NM_134102.1	***phospholipase A1 member A (Pla1a)***
AF162713.1	***phospholipase A2, group V (Pla2g5)***

Table 2 *(continued)*

GenBank	Gene title
Metabolism	
AK009249.1	***RIKEN cDNA 2310009E04 gene (2310009E04Rik)***
BC020489.1	***RIKEN cDNA 2310016F22 gene (2310016F22Rik)***
NM_011435.1	***superoxide dismutase 3, extracellular (Sod3)***
Protein modification	
BC016526.1	N-myristoyltransferase 1 ***(Nmt1)***
BI525140	plectin 1 (Plec1)
BC016187.1	RIKEN cDNA 2010008E23 gene ***(2010008E23Rik)***
AV002340	***RIKEN cDNA 4833442J19 gene (4833442J19Rik)***
Protein biosynthesis	
NM_026729.1	***immature colon carcinoma transcript 1 (Ict1)***
AK012225.1	mitchondrial ribosomal protein S7 ***(Mrps7)***
AK002757.1	mitochondrial ribosomal protein L12 ***(Mrpl12)***
BB041267	mitochondrial ribosomal protein L19 ***(Mrpl19)***
NM_011885.1	***mitochondrial ribosomal protein S12 (Mrps12)***
NM_025440.1	***mitochondrial ribosomal protein S16 (Mrps16)***
M58566.1	zinc finger protein 36, C3H type-like 1 ***(Zfp36l1)***
Protein folding	
BC025552.1	***AHA1, activator of heat shock protein ATPase homolog 1 (yeast) (Ahsa1)***
BC017161.1	***Dnaj (Hsp40) homolog, subfamily B, member 4 (Dnajb4)***
Protein degradation	
AK009033.1	Brca1 associated protein 1 ***(Bap1)***
NM_011189.1	proteasome (prosome, macropain) 28 subunit, alpha ***(Psme1)***
NM_011190.1	proteasome (prosome, macropain) 28 subunit, beta ***(Psme2)***
Signal transduction	
BC019379.1	***G protein-coupled receptor kinase 5 (Gprk5)***
BI645481	***guanine nucleotide binding protein, alpha 13 (Gna13)***
BC003980.1	protein tyrosine phosphatase, non-receptor type 11 ***(Ptpn11)***
NM_009105.1	Ras suppressor protein 1 ***(Rsu1)***
NM_019662.1	***Ras-related associated with diabetes (Rrad)***
AF215669.1	***regulator of G-protein signaling 3 (RGS3)(C2PA) (Rgs3)***
Transcription	
AK004254.1	***ankyrin repeat domain 46 (Ankrd46)***
AI852593	bromodomain PHD finger transcription factor ***(Bptf)***
NM_007970.1	enhancer of zeste homolog 1 (Drosophila) ***(Ezh1)***
BM232562	***feminization 1 homolog b (C. elegans) (Fem1b)***
BC016637.1	general transcription factor IIB ***(Gtf2b)***
BC004625.1	***neural precursor cell expressed, developmentally down-regulated gene 8 (Nedd8)***
Transport	
NM_007899.1	***extracellular matrix protein 1 (Ecm1)***
BC008525.1	***golgi SNAP receptor complex member 2 (Gosr2)***
BC011470.1	phosphatidylinositol binding clathrin assembly protein ***(Picalm)***
BC014701.1	potassium voltage-gated channel, shaker-related subfamily, beta member 1 ***(Kcnab1)***
AK016883.1	RIKEN cDNA 4933425K02 gene ***(4933425K02Rik)***
AF297098.1	***six transmembrane epithelial antigen of the prostate 1 (Steap1)***
Unknown	
NM_007786.1	casein kappa ***(Csn3)***
BC021637.1	CD68 antigen ***(Cd68)***
BE853170	***cDNA sequence BC006779 (BC006779)***
NM_025779.1	coiled-coil domain containing 109B ***(Ccdc109b)***
NM_007793.1	cystatin B ***(Cstb)***
BE571790	***epithelial membrane protein 2 (Emp2)***
NM_010500.1	immediate early response 5 ***(Ier5)***
NM_011150.1	***lectin, galactoside-binding, soluble, 3 binding protein(Lgals3bp)***
NM_024194.1	leucine rich repeat containing 40 ***(Lrrc40)***
AV010467	LIM domain containing 2 ***(Limd2)***
AF263458.1	***placenta-specific 8 (Plac8)***
BQ175991	***progesterone receptor membrane component 2 (Pgrmc2)***
BC009150.1	RAB, member of RAS oncogene family-like 5 ***(Rabl5)***
NM_133231.1	regulatory factor X-associated protein ***(Rfxap)***
BC025602.1	***reticulocalbin 3, EF-hand calcium binding domain (Rcn3)***
BC026936.1	RIKEN cDNA 1110005A03 gene ***(1110005A03Rik)***
AK015585.1	***RIKEN cDNA 2610027L16 gene (2610027L16Rik)***
NM_026481.1	RIKEN cDNA 2700055K07 gene ***(2700055K07Rik)***

Table 2 *(continued)*

GenBank	Gene title
Unknown	
AY043488.1	selenoprotein M ***(Selm)***
BC022145.1	***transmembrane protein 106A (Tmem106a)***
BE225838	WD repeats and SOF domain containing 1 ***(Wdsof1)***

Note: These genes were assigned to cluster 1. Genes showing downregulated expression in necrosis are grouped according to function, and gene symbols are indicated in parentheses. The bold italic-lettered genes were those downregulated > 1.5-fold ($p < 0.001$) in F28-7 cells compared with those in F28-7-A after treatment with FUdR for 16 h.

Northern blot analysis in terms of its quantitative power and sensitivity. Indeed, in the present analysis, the *Myc* mRNA expression did not show a clear upregulation from 8 to 16 h. These expression patterns obtained by the microarray data are given in Supplementary Data (Supplementary Fig. 5). These observations indicate the competency of the microarray data.

Of particular interest in the changes of the expression patterns were those of a cluster of HSP90 chaperone complex-related genes, particularly because HSP90 is a current focus of attention as an anticancer-drug target [19] and is suspected to be involved in TNF-induced necrosis and apoptosis [16].

FUdR induces release of cytochrome c from mitochondria in apoptosis, but not in necrosis

A number of apoptosis-related genes involved in mitochondria-dependent apoptosis signaling exhibited differentially expressed patterns in the observed necrosis and apoptosis. These genes, including *Bcl10*, *Bid*, and *Glrx2*, showed downregulated expression in the necrosis as compared to the apoptosis. Therefore, we investigated mitochondrial events, i.e., changes in mitochondrial membrane potential and release of cytochrome *c* accompanying the treatment with FUdR.

First, we analyzed changes of mitochondrial membrane potential in F28-7 and F28-7-A cells using the uptake of Rhodamine 123 as a probe (Fig. 2). At 24 h of the treatment, the pattern changes from the 0-time control were similar in F28-7 and F28-7-A cells. In both cells, the uptake of Rhodamine 123 was decreased (left-side shift in the dye content). These observations indicate that the mitochondrial membrane potentials of these cells undergo changes quite similar to each other during the FUdR treatment.

Next, we investigated whether FUdR induces release of cytochrome *c* from mitochondria. As shown in Fig. 3, a release of cytochrome *c* into cytoplasm and nucleus was detected for F28-7-A but not for F28-7 cells, thus confirming an alteration in the apoptosis-related genes.

Inhibition of HSP90 in F28-7 cells causes a shift from necrosis into apoptosis

Microarray analysis also revealed differentially expressed genes in necrosis and apoptosis among those involved in the HSP90 chaperone complex. These genes, including *Hsp110*, *Ahsa1*, and *Dnajb4*, are associated with stress response and protein folding. However, the mRNA expression levels of the HSP90 isoforms, HSP90 alpha and HSP90 beta, showed no significant changes in the microarray analysis. Therefore, we considered that the HSP90 functions may differ between F28-7 and F28-7-A cells. To investigate the effect of inhibiting the HSP90 functions, we performed a DNA fragmentation assay in F28-7 and F28-7-A cells treated with a combination of the HSP90 inhibitor GA and FUdR. As shown in Fig. 4a, oligonucleosomal DNA fragmentation was induced by this combination treatment in F28-7 cells. On the other hand, in F28-7-A cells, such oligonucleosomal DNA fragmentation was induced by treatment both with FUdR alone and with the combination of GA and FUdR (Fig. 4a). These observations therefore suggest that the HSP90 participates in executing the process of necrosis.

We also observed morphological changes in F28-7 cells treated with the combination of GA and FUdR. FUdR alone induced the cytoplasmic swelling, a hallmark for necrosis, whereas the combination of GA and

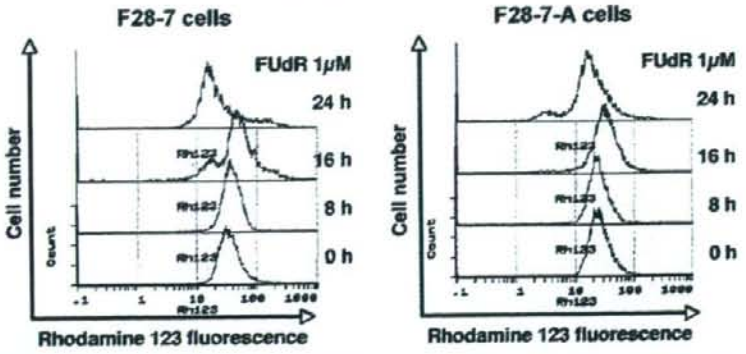

Fig. 2. Change of mitochondrial membrane potential in F28-7 and F28-7-A cells treated with FUdR. F28-7 and F28-7-A cells were treated with 1 μM FUdR for 0, 8, 16, or 24 h, and the mitochondrial membrane potential was assessed with Rhodamine 123, a membrane-permeant mitochondria-specific tracer dye, using flow cytometry. Loss of mitochondrial membrane potential causes release of Rhodamine 123 from mitochondria, resulting in decreased Rodamine 123 intensity. Three independent experiments were performed and the results shown represent those obtained in one experiment. Two other experiments generated similar results.

FUdR induced a typical apoptotic morphology, the membrane blebbing and the formation of apoptotic bodies (Fig. 4b). In the case of F28-7-A, typical apoptotic phenomena were observed in treatments with FUdR alone, and with the combination of FUdR and GA (data not shown).

To obtain further evidence for this remarkable phenomenon, we performed an immunofluorescence study. As shown in Fig. 5, this study also showed the release of cytochrome *c* in F28-7 on treatment with the combination of GA and FUdR. As expected, the cytochrome *c* release was not observed in F28-7 cells treated with GA or FUdR alone.

Discussion

In the present study, we investigated the gene expression profiles of FUdR-induced necrosis and apoptosis using cDNA microarray technology and demonstrated clear differences between these profiles. In this analysis, 215 genes were identified as differentially expressed in necrosis and apoptosis induced by FUdR, and the gene expression patterns differed significantly between F28-7 and F28-7-A cells treated for 0, 4, 8, and 16 h (Fig. 1). Among these differentially expressed genes were those involved in a variety of intracellular signaling pathways, for example, apoptosis, chromatin modification, cytoskeleton organization, and protein folding (Tables 1 and 2). These 215 genes were classified into two clusters according to the gene expression patterns; a cluster of genes upregulated in the FUdR-induced necrosis compared to those in the induced apoptosis, and another cluster downregulated in the necrosis compared to those in the apoptosis. In addition, the microarray analysis revealed that already in the untreated stage (0-time controls), a number of genes are differentially expressed between F28-7 and F28-7-A cells. Therefore, the differences in the gene expression at 0 h may appear to determine the FUdR-induced necrosis and apoptosis. The differencies in these sister cells may also be a result of mutation(s), although undiscovered yet, in the upstream of these genes. Another possible mechanism, however, seems more attractive to us. First, in these differentially expressed genes, over 90% had similar changing patterns during the FUdR treatment. Furthermore, some genes that are differentially or similarly expressed in the untreated stage of F28-7 and F28-7-A cells show quite different patterns of expression changes during the subsequent FUdR treatment. Importantly, our previous work revealed that newly synthesized proteins are required for the FUdR-induced death of F28-7 cells. Thus, cycloheximide, an inhibitor of protein biosynthesis, added to the culture medium at a stage when new protein synthesis began to start, caused a strong inhibition of the FUdR-induced cell death [7]. Therefore, the necrosis and apoptosis that occurred seemed to be regulated by FUdR-inducible genes, requiring newly synthesized proteins. Taken together, we hypothesized that not only the inherent differences in the gene expressions of F28-7 and F28-7-A, but also the dynamic changes in the expressions during the FUdR treatment are important in determining the mode of the cell death for these sister cells.

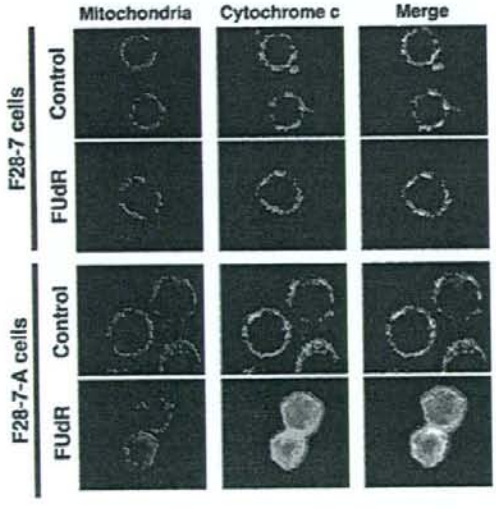

Fig. 3. FUdR induced release of cytochrome *c* from mitochondria in F28-7-A cells, but not from F28-7. Immunofluorescence studies in F28-7 and F28-7-A cells. Cells plated on glass coverslips were treated with 1 μM FUdR for 0 (control) or 16 h. After fixation, the subcellular distribution of cytochrome *c* was visualized with anti-cytochrome *c* antibodies (green) using a fluorescence microscope. Mitochondria were stained with MitoTracker Red CMXRos (red). The results shown are those in an experiment out of three independent experiments (all of them gave similar results).

We identified many apoptosis-related genes that showed differential expressions in necrosis and apoptosis induced by FUdR. These genes, including the BCL-2 family such as *Bcl10*, *Bid*, and *Glrx2*, are involved in the mitochondria-dependent apoptosis pathway. Recent reports have shown that mitochondria play a role in mediating both apoptosis and necrosis [20–22]. In apoptosis and necrosis, the mitochondrial permeability transition (mPT), which leads to mitochondrial membrane disruption accompanying a total dysfunction, is considered to be one of the key events [22,23]. Also, release of cytochrome *c* from mitochondria is a major event during apoptosis [24–26]. Once released into the cytoplasm, cytochrome *c* is known to form a molecular

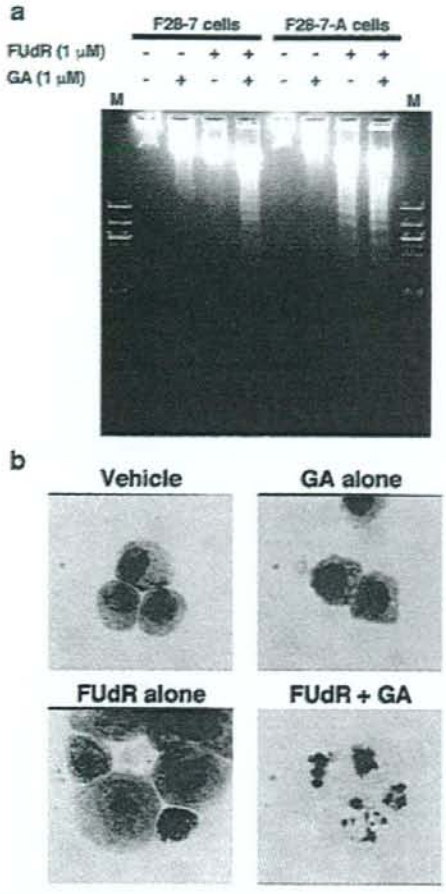

Fig. 4. A combination of FUdR and GA induces oligonucleosomal DNA fragmentation and apoptotic cell morphology in F28-7 cells. (a) Oligonucleosomal DNA fragmentation was detected using 2% agarose gel electrophoresis followed by ethidium bromide staining. F28-7 and F28-7-A cells were treated with vehicle (0.1% DMSO), 1 μM GA alone, 1 μM FUdR alone, or 1 μM FUdR plus 1 μM GA for 21 h. Lane M shows 123 bp ladder size markers. The results are representative of four independent experiments. (b) Morphological changes were observed by Giemsa staining. F28-7 cells were treated with vehicle (0.1% DMSO), 1 μM GA alone, 1 μM FUdR alone, or 1 μM FUdR plus 1 μM GA for 21 h. The results shown are those of an experiment from three independent experiments (all of them gave similar results).

complex with Apaf-1, which then activates a caspase cascade leading to many apoptotic events [24–26]. In many forms of apoptosis, BH3-domain-containing proteins of the BCL-2 family transduce apoptotic signals to the mitochondria, and induce cytochrome *c* release [27]. We showed that the mitochondrial membrane potential decreases in the FUdR-induced necrosis and apoptosis in a time-dependent manner very similar to each other (Fig. 2). However, release of cytochrome *c* from mitochondria into the cytoplasm and nucleus was found in the apoptosis but not in the necrosis (Fig. 3). A recent report suggests that the nuclear accumulation of cytochrome *c* may be directly involved in the remodeling of chromatin [28]. Therefore, we consider that the cytochrome *c* release may be important in the apoptosis induced by FUdR. Our working hypothesis that the dynamic expression changes must be the cause of the shift in the cell death mode is in agreement with this behavioral change of mitochondria.

Interestingly, HSP family and related genes showed differential expression patterns in these cells. These genes, including *Hsp110*, *Dnajb4*, and *Ahsa1*, are involved in the HSP90 chaperone complex. In particular, AHA1 is an activator of the HSP90 ATPase activity, which plays a key role in the regulation of ATP-dependent HSP90 chaperone activity [29–32]. HSP90 is one of the more abundant HSPs, and because it regulates the stability and function of a unique complement of signal transduction proteins, this chaperone is involved in a variety of important biological processes including hormone signaling, cell cycle control, development, and cell death [13–19]. The HSP90 chaperone machine is driven by ATP binding and hydrolysis [33–35]. Its activity is regulated by cochaperones such as AHA1, HSP72, CDC37, p23, CHIP, and immunophilins [36,37]. Therefore, it may be expected that HSP90 ATPase activity differs between F28-7 and F28-7-A cells. To investigate the involvement of HSP90 in FUdR-induced necrosis and apoptosis, we used an HSP90 inhibitor, GA. This naturally occurring ansamycin antibiotic GA binds to a conserved binding pocket in the amino-terminal domain of HSP90 [38,39], inhibiting ATP binding and ATP-dependent HSP90 chaperone activity [33–35]. As shown above, inhibition of HSP90 caused a shift from FUdR-induced necrosis to apoptosis in F28-7 cells (Figs. 4a and b). Berghe et al. reported that inhibition of HSP90 function reverts TNF-induced necrosis to apoptosis [16]. These results suggest that HSP90 is crucial to necrosis. However, the *Ahsa1* gene showed downregulated expressions in F28-7 cells as compared to F28-7-A during the entire period of the FUdR treatment (Supplementary Fig. 2). Also, the mRNA expression levels of HSP90 isoforms, HSP90 alpha and HSP90 beta, did not significantly change as revealed by our microarray analysis. Furthermore, we measured the protein expression levels of the HSP90 isoforms (HSP90 alpha and HSP90 beta) and AHA1 by proteome analysis using two-dimensional gel electrophoresis and mass spectrometry. The results indicated that the protein expression levels of HSP90 isoforms were not significantly different between F28-7 and F28-7-A cells, in agreement with the similarity in their gene expression levels. In contrast, however, the AHA1 protein expression level was found to be downregulated in F28-7

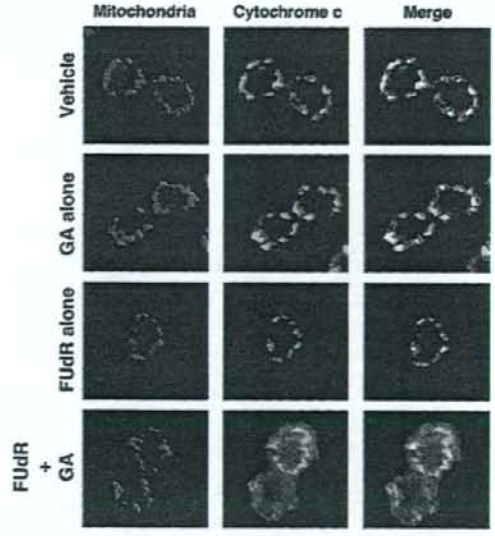

Fig. 5. A combination of FUdR and Hsp90 inhibitor GA induces release of cytochrome *c* from mitochondria in F28-7 cells. F28-7 cells were treated with vehicle (0.1% DMSO), 1 μM GA alone, 1 μM FUdR alone, or 1 μM FUdR plus 1 μM GA for 16 h. Immunostaining was performed using anti-cytochrome *c* antibody (green). Mitochondria were stained with MitoTracker Red CMXRos (red). The results shown are those of an experiment from three independent experiments (all of them gave similar results).

cells compared to that in F28-7-A cells (details to be published elsewhere). One possibility is that in F28-7 cells AHA1 may be under a negative feedback control at its transcriptional step by the enhanced activity of HSP90.

In addition, we demonstrated that a release of cytochrome c from mitochondria to cytoplasm and nucleus was inducible in F28-7 cells by a combination of GA and FUdR (Fig. 5). This finding suggests that HSP90 may play a role prior to the release of cytochrome c in the FUdR-induced necrosis and apoptosis. Taken together, these results permit us to speculate that in F28-7 cells the apoptotic pathway is blocked by HSP90 and/or HSP90 chaperone complex constructs (such as AHA1 and HSP110), whereas in F28-7-A cells this block has been overcome. It appears important to explore further the roles of HSP90 and cochaperone AHA1 in necrosis and apoptosis.

As noted under Results, previous reports from other laboratories described FUdR-mediated changes in genes for thymidylate synthase [40], uracil-DNA glycosylase [41], and thymidine kinase [41]. However in our present survey, we observed no significant changes in those genes. This discrepancy could have resulted from differences in the cell types and in the analytical methods.

As described above, microarray analysis revealed differently expressed genes (see bold italic-lettered genes in Tables 1 and 2). Most of these genes are for the first time revealed as differently expressed in necrosis and apoptosis. Interestingly, some genes were upregulated in the FUdR-induced necrosis. Participation of these genes in necrosis has not been reported previously. Furthermore, we analyzed gene expression changes in apoptotic conditions; namely F28-7 cells treated with a combination of FUdR and GA, and F28-7-A cells treated with FUdR alone. The results indicated that genes, involving *Serpinb2*, *Sele*, and *Egr1*, are downregulated under the apoptotic conditions induced (details to be published elsewhere). It would be interesting to explore the effect of knocking down these genes (for example, with siRNAs) to see whether apoptosis is inducible.

The possible new roles supposedly assignable to HSP90 seem to warrant further studies. For example, agents other than FUdR may also exhibit a similar association with HSP90.

In conclusion, we revealed the gene expression profiles of necrosis and apoptosis induced by FUdR and proposed possible mechanisms associated with the cell death. Our present work should contribute to a better understanding of the molecular mechanisms regulating necrosis and apoptosis. Also, we suggest that HSP90 plays a key role in the regulation of necrosis and apoptosis induced by FUdR.

Materials and methods

Reagents, antibodies, and cell culture

5-Fluoro-2′-deoxyuridine and geldanamycin were obtained from Sigma. Rhodamine 123, 4′,6-diamidino-2-phenylindole dihydrochloride (DAPI), and MitoTracker Red CMXRos were from Invitrogen. The antibodies anti-cytochrome c and anti-mouse IgG (containing Alexa 488) were from Calbiochem and Invitrogen, respectively. FUdR was stored as 2 mM stocks in HPLC grade water at −20 °C. GA was stored as 2 mM stocks in DMSO at −20 °C with protection from light.

Original-type F28-7 clones of mouse mammary tumor FM3A cells and variant F28-7-A cells used in the study have been described previously [12]. The cells were cultured in ES medium (Nissui Pharmaceuticals) supplemented with 2% fetal bovine serum (Gibco) and 0.03% L-glutamine (Wako) in a humidified atmosphere with 5% CO_2 at 37 °C. Under these conditions, the doubling time of both F28-7 and F28-7-A cells was approximately 12 h.

Microarray analysis and data statistics

For microarray analysis, F28-7 and F28-7-A cells at 2×10^5 cells/mL were treated with 1 μM FUdR for 0, 4, 8, and 16 h. Total RNA was extracted by using QIAshredder spin columns and an RNeasy Mini kit as described by the manufacturer (QIAGEN). Biotin-labeled cRNA and the hybridization cocktail were prepared using a One-Cycle Target Labeling kit and Control Reagents as described in the GeneChip Expression Analysis Manual (Affymetrix). Briefly, total RNA was converted to double-stranded cDNA using an oligo$(dT)_{24}$ primer containing a T7 promoter sequence. The resulting cDNA was transcribed into biotin-labeled cRNA using T7 RNA polymerase and biotinylated ribonucleotides. The cRNA product was purified, fragmented, and placed in a hybridization cocktail. The hybridization cocktails were added to GeneChip Mouse Expression Array 430A (Affymetrix) in the GeneChip Hybridization Oven 640 under constant rotation at 60 rpm at 45 °C for 16 to 18 h. After the hybridization, GeneChips were washed and stained with GeneChip Fluidics Station 450 (Affymetrix), and scanned with a GeneArray 2500 Scanner (Agilent Technologies). Pixel size was set to 3 μm, filter wavelength to 570 nm, and scan number to 2. Other parameters were set according to the details specified by Affymetrix for the GeneChip Mouse Expression Array 430 A. Scanned GeneChip images were analyzed using GeneChip Operating Software (GCOS) ver. 1.4. (Affymetrix). To ensure the reproducibility of the microarray data, three independent analyses were performed with the GeneChip Mouse Expression Array 430A, which contains 22,600 probe sets and can be used to analyze the expression level of ~14,000 known mouse genes. The concentrations of total RNA and biotin-labeled cRNA were determined by ultraviolet absorbance. The quality and integrity of the total RNA and fragmented cRNA were confirmed using the Bioanalyzer Experion electrophoresis system (Bio-Rad).

Raw data were analyzed using Array Assist ver. 5.2. software (Stratagene). Probe sets of all 24 arrays (three arrays per one time point) were normalized by Affymetrix Microarray Suite MAS 5.0 (for details see www.affymetrix.com), and genes of absence calls across all arrays were removed; then probe signal values were transformed to a logarithmic scale. After this transformation, probe sets were subjected to ANOVA [42,43], setting P values below 0.001 after application of the Bonferroni correction [44]. Genes with P values smaller than 0.001 were selected for further analysis. Unsupervised hierarchical clustering using the Pearson correlation with the average linkage rule was performed on the statistically significant probe sets [45,46]. Data are graphically presented as heat maps in which signal intensity is represented by a color gradient.

Functional classification of the genes was based on gene ontology categories established by the Gene Ontology Consortium (http://www.geneontology.org).

Assessment of mitochondrial membrane potential

To examine changes in the mitochondrial membrane potential, F28-7 and F28-7-A cells were treated with Rhodamine 123 (final concentration 5 μM), a membrane-permeant mitochondria-specific tracer dye, for 15 min at 37 °C in a CO_2 incubator. Then, 2×10^5 cells were centrifuged at 250 g, 5 min, 4 °C, and resuspended in phosphate-buffered saline (PBS). Mitochondrial membrane potential was analyzed by a Beckman Coulter Epics XL flow cytometry.

Immunofluorescence

F28-7 and F28-7-A cells plated on glass coverslips were treated individually with 1 μM FUdR. Also, F28-7 cells were treated with vehicle (0.1% DMSO), 1 μM GA alone, 1 μM FUdR alone, or 1 μM FUdR plus 1 μM GA. Cells were loaded with MitoTracker Red CMXRos (200 nM), a mitochondria selective dye, for 15 min at 37 °C in a CO_2 incubator. Cells were rinsed three times with PBS and then fixed with 4% paraformaldehyde in PBS, for 15 min at room temperature. After fixation, cells were permeated with 0.2% Triton-X, for 5 min at room temperature, and rinsed three times with PBS. Cells were then treated with blocking solution (0.5% bovine serum albumin (BSA) in PBS) for 30 min at room temperature and incubated with monoclonal anti-cytochrome c antibody diluted to 3.3 μg/mL in blocking solution for 1 h at room temperature. Excess antibody was removed by washing the coverslips three times with PBS for 5 min. The secondary antibody, anti-mouse IgG containing Alexa 488, diluted 1:100 in blocking solution, was probed for 30 min at room temperature. Staining of the nucleus was accomplished by incubation with DAPI (1 μg/mL) for 1 min after antibody treatment. Coverslips were then rinsed three times with PBS for 5 min and mounted onto microscope slides using PermaFluor Aqueous Mounting Medium (Shandon) and analyzed using an Olympus BX61 fluorescence microscope equipped with appropriate fluorescence filters.

Morphological change

To characterize the morphology of F28-7 cells after treatment with vehicle (0.1% DMSO), 1 μM GA alone, 1 μM FUdR alone, or 1 μM FUdR plus 1 μM GA, cells were fixed with methanol and stained with Giemsa stain solution (Wako) as described in the manufacturer's instructions. Cell morphology was observed by an Olympus BX50 light microscopy.

DNA fragmentation assay

DNA samples for detection of apoptotic oligonucleosomal DNA fragmentation were prepared as described previously [12]. DNA fragmentation was detected using 2% agarose gel electrophoresis followed by ethidium bromide staining.

Acknowledgments

The authors thank Hikoya Hayatsu (Faculty of Pharmaceutical Sciences, Okayama University) for helpful discussions. This research was partly supported by the Ministry of Education, Culture, Sports, Science, and Technology for Exploratory Research (18659029, Y.W.).

Appendix A. Supplementary data

Supplementary data associated with this article can be found, in the online version, at doi:10.1016/j.ygeno.2008.02.002.